BNL-52450
FORMAL REPORT

# TECHNICAL EVALUATION REPORT

# SEISMIC ANALYSIS OF THE PAR POND DAM
## Study of Slope Failure and Liquefaction

**Prepared by**

**N. Simos and M. Reich**

**July 1994**

## DISCLAIMER

## ABSTRACT

Stability concerns of the Par Pond Dam, an embankment structure in the Savannah River Site complex, resulted in a comprehensive evaluation of the state of its integrity.

Specifically, excessive seepage through the embankment, slope failure due to an earthquake event as well as liquefaction potential of the embankment and the foundation are addressed and the potential of failure is evaluated.

Lastly, remedial benefits of the addition of a berm structure are also assessed.

## Executive Summary

A comprehensive study to assess the impact of a seismic event on the Par Pond Dam has been undertaken. Concerns of dam stability stem from the presence of a *weak* soil layer beneath the embankment of the dam.

Due to the complexity of the physical problem and uncertainties in the true values of key parameters (such as soil damping, soil relative density etc.), assessments of the failure potential of the dam are made through parametric evaluations to provide estimates of the susceptibility to failure due to either liquefaction or slope sliding.

The overall evaluation procedure involves several steps each of which addresses a specific aspect of dam stability. Results of these various steps are linked and assessments of the stability are made. Specifically, the analysis proceeds with: (a) the determination of the basic physical parameters (density, shear modulus etc.) from available or extrapolated field data (such as standard penetration test results and soil permeability), (b) the evaluation of the *steady-state* stress conditions corresponding to soil dead weight and reservoir water, (c) the calculation of the seepage forces and consequently the initial *effective* stresses, (d) the evaluation of the potential for slope sliding failure for static conditions and for static conditions amplified to simulate a seismic input using *a simplified* method to estimate slope stability, (e) the calculation of the dynamic response of the dam and its foundation to earthquake excitations and (f) the evaluation of the failure potential based on the calculated dynamic and *steady-state* results.

The dynamic response of the Par Pond Dam is evaluated by treating the saturated soil as a two-phase medium. This approach involves the determination of both the intergrannular stresses and the pore pressures in the medium for the entire duration of the earthquake. Even though the formulation is a linear description of the constitutive response of the soil-water medium, important conclusions concerning the dam stability are deduced.

The failure potential of the dam for a Charleston-like earthquake with a peak ground acceleration of 0.11 g, considered to be representative of the site, is estimated. The analysis indicated that, (1) for competent soil property assumptions the safety factor against slope failure remains above 1.0 and (2) for the same dynamic event and under extremely conservative assumptions of soil damping and strength, liquefaction failure can be trig-

gered at the bottom of the weak layer.

In further analyses the benefits of a berm placed downstream of the dam were evaluated. Presence of the berm reduced the potential for liquefaction and shifted the critical zone downstream. Additional studies to assess the behavior of the weak sand under the increased effective stress field produced by the berm must be performed to confirm the positive effect.

Lastly, based on analysis results, stronger ground motions combined with the conservative estimates of the key soil properties, reduce the safety factors for both modes of failure below tolerable limits.

# 1. INTRODUCTION

The Par Pond Dam is an embankment structure within the Savannah River Site complex in South Carolina built by the Army Corps of Engineers in the late 1950s. The purpose of the dam was to provide recirculating cooling water for the P and R reactors. Figure 1.1 shows the geographical location of the Par Pond Dam and Figure 1.2 is a representation of the cross section of the embankment and the foundation layers. On the basis of design and safety criteria the dam was classified a **high-hazard** structure. The height of the dam is 65 feet and the width 4,500 feet. The design elevation of the crest is 210 feet with a spillway at 200 ft. The pool level has typically been maintained at the spillway level.

Excessive seepage was noted soon after the dam was built, but corrective action eliminated that problem. In March of 1991,however, a depression was noted at the downstream face prompting a series of investigations to assess the condition of the dam and its susceptibility to failure. In that process, a series of soil tests were conducted for both the embankment and the foundation layers.These tests indicated that a layer of loose sands exists deep in the foundation of the dam which had not been accounted for in the original dam design.

A *screening study* by DOE consultants raised concerns regarding seismic stability steming from this seemingly *weak layer* of foundation soil. Along with the excessive seepage and embankment slope failure, the potential for liquefaction failure was also added to the concerns.

While further penetration tests were recommended, general concepts for remediation were proposed by the DOE consultants ranging from the stiffening of the weak soil layer to construction of a downstream berm.

**EH** requested that **BNL** perform an independent safety evaluation of the Par Pond Dam. In performing this task all possible challenges to the dam integrity were to be considered. This included the potential for excessive seepage, embankment slope instability and and liquefaction failure.

The BNL analysis consists of a series of steps each of which addresses a specific aspect of dam integrity. Specifically, the following important

parameters were assessed:

- Seepage forces generated by the flow of water through the dam and its foundation.
- Present soil conditions within the embankment that dictate both the amount of seepage as well as the inherent strength of the structure.
- Driving forces along potential failure surfaces that determine the level of safety against slope sliding and failure during an earthquake.
- The influence of critical soil parameters and their impact on the dynamic response and structural integrity of the dam.
- The profile and the condition of the soil constituting the foundation of the dam and its potential to liquefy.

This complete matrix of critical system parameters is addressed with emphasis given to the coupling between them. Subsequently, on the basis of the computed dam response the potential for failure is estimated. The slope failure potential in the embankment is assessed in terms of a safety factor against sliding along a failure surface while the liquefaction potential is measured against the ability of the soil in the embankment and the foundation to withstand an anticipated level of shear stress during a seismic event. It should be emphasized that while basic procedures exist in assessing such failure potentials, they fail to (a) represent the soil as a two phase medium and (b) implement seismic inputs in the form of acceleration time histories.

Initial conservative estimates of safety are obtained by utilizing the slope stability program REAME. This program is based on the quasi-static analysis of slopes and treats the soil as a single phase medium. Subsequent analyses are performed using the POROSLAM 2-D finite element program which allows two-phase soil representation and accepts a time history variation of the ground acceleration.

The stability of the Par Pond Dam and its susceptibility to failure was evaluated taking proper consideration of the important coupling existing between the various steps. It is important to note that results from one phase of the evaluation provide important information for the next phase. A profile of these analysis steps in their proper order is provided below:

i. *Screening* of the susceptibility of the dam to slope failure is first performed using the REAME (Rotational Equilibrium Analysis of Multi-layered Embankments) program. The code provides conservative first estimates of the safety margins regarding slope stability of the dam. Important parameters that impact on the safety criteria are the soil frictional angle and cohesion. Safety factors against sliding along assumed failure surfaces through the embankment and the foundation layers are evaluated for a range of soil parameters that seem reasonable. The analysis considers both the steady-state (static) and a pseudo-static (to account for seismic effects trough a seismic coefficient) loadings. Based on the results, the impact of each parameter is assessed.

ii. *Seepage Forces* are evaluated by considering the flow of water through the dam. The steady state pore water pressure field is evaluated through a finite element seepage analysis using the ANSYS general purpose program. The pore pressure field is an important input in the determination of the steady state stress distribution. The pore water supports a fraction of the static stresses reducing the intergranular soil stresses. The analysis also provides the location of the phreatic surface.

iii. *The steady-state stress* condition in the embankment and the foundation layers is evaluated. This *in-situ* stress field, resulting from the action of the reservoir water and the soil overburden, is key to the definition of stability of the dam. With elastic soil properties extrapolated from test data for the site and using finite element analysis, the stress field in the embankment and the foundation caused by the reservoir load and the overburden is evaluated. The effective stress field that exists prior to a dynamic event is evaluated by incorporating the calculated pore pressure field. Effective stress is the difference between the soil overburden stress and the pore water pressure. Through the same analysis the *steady-state* shear stresses are also evaluated. Each of these stress calculations is performed using the ANSYS code.

iv. *The dynamic response* of the embankment/foundation system to earthquake loadings is evaluated next. This seismic analysis provides the stress time histories throughout the structure caused by the design earthquake. This stress history combined with the steady state effective stress field calculated in step **iii** become the basis of the safety

assessment for both slope stability and liquefaction. The design seismic input is a CHARLESTON-like earthquake of intensity **0.11g**. The dynamic response is evaluated using the POROSLAM code which is a linear analysis program that treats the soil as a two-phase medium. The theoretical basis of this program is described in a later section.

v. *Evaluation of Failure Potentials.* Based on the *in-situ* stress conditions and its dynamic response the margins of safety against failure in the following modes are evaluated to assess the capacity of the dam to withstand the design earthquake.

a. *Slope Stability :* Along various surfaces where sliding can occur, the dynamic factors of safety are computed and the most critical or potential failure surfaces are identified. This process is performed using extrapolated values of soil cohesion and frictional angle. Since there are uncertainties in the exact values of these two parameters, the safety factors are calculated considering a parametric variation of them.

b. *Liquefaction :* Failure of this mode occurs when the embankment and the foundation liquefy during a dynamic event. The driving force in the liquefaction process is the dynamic (cyclic) shear stress generated in the soil layers. The resisting force is the shearing strength of the soil. This strength can be assessed by bore hole testing and correlation with laboratory test results. The dynamic shear stress is provided by the POROSLAM analysis while the **standard penetration test results** along with the predicted initial (steady-state) effective stress provide the shear strength of the entire cross section of the embankment and the foundation layers.

c. *Slope Failure/Liquefaction Connection:* The possibility that a localized liquefaction condition can trigger a slope failure is also examined. It is possible that in the lower foundation layers where dynamic shear stresses are at a maximum, portions of the weak layer will liquefy. Localized liquefaction does not necessarily mean loss of strength in the entire layer but it could very well mean a reduction of the safety factor over a potential failure surface transversing the liquefied spot. Such a reduction could precipitate sliding failure. In order to evaluate the coupling of the two failure modes, the safety factor against slope failure is re-evaluated taking into account the change in cohesion and frictional angle that occurs within the liquefied zone.

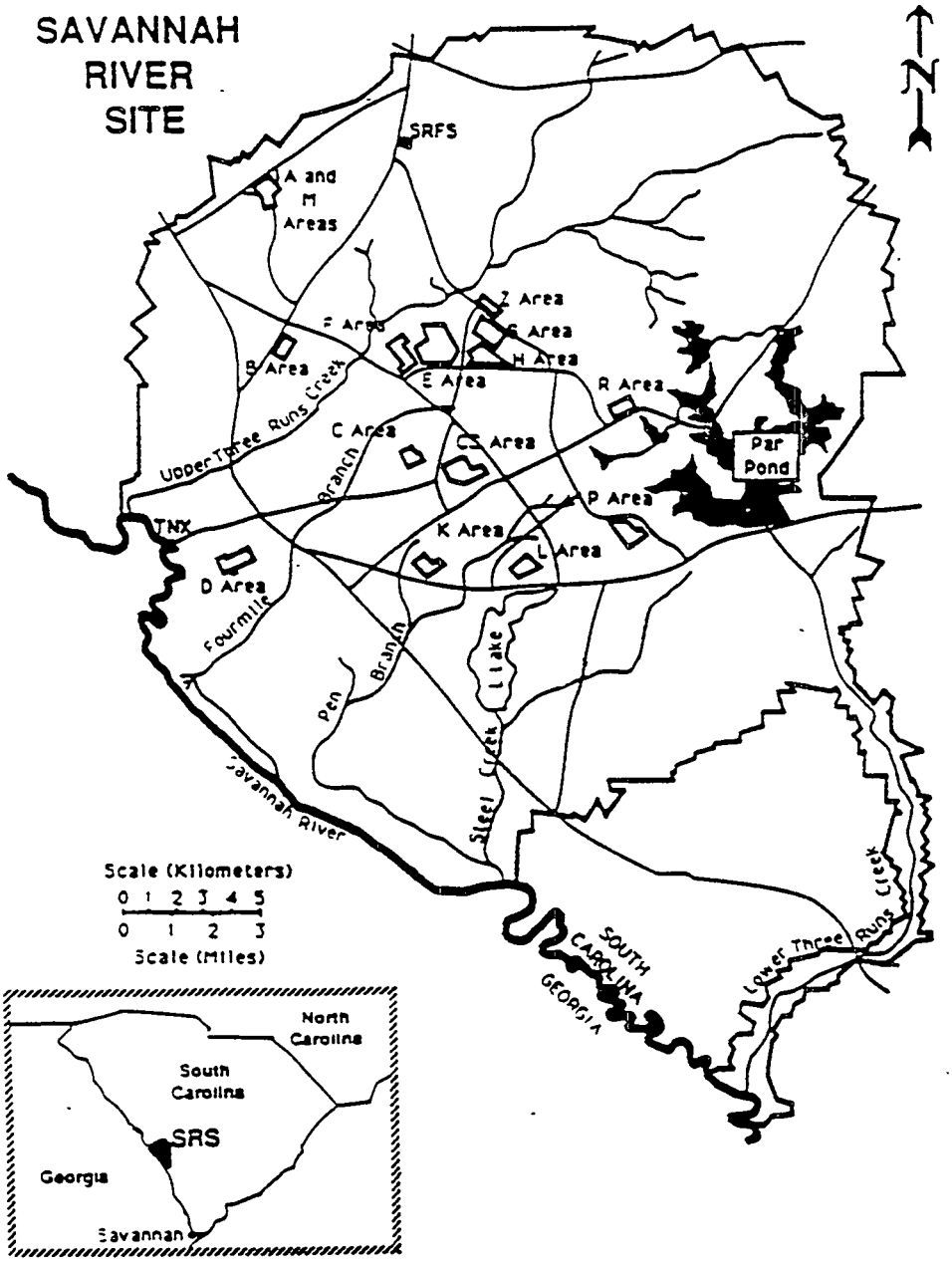


**Figure 1.1** Geographical Location Of the Par Pond Dam

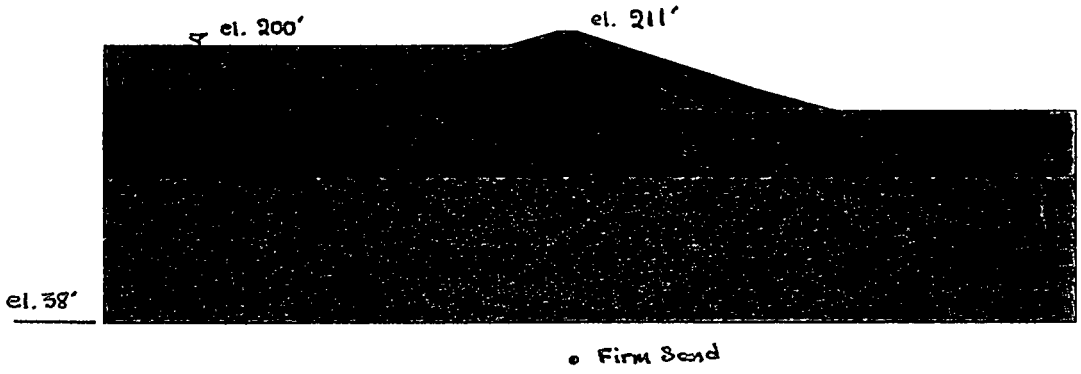


**Figure 1.2** Cross Section of Par Pond Embankment and Foundation

# 2. SITE DESCRIPTION

Over the years a number of subsurface explorations have been undertaken to determine the soil conditions in the foundation layers as well in of the constructed embankment. During the design phase of the Par Pond Dam the foundation layer was tested with borings by the Corps of Engineers (1957). Twenty years later (1978) borings were again performed to assess the condition of the downstream section of the embankment. The most extensive site exploration took place in 1991 and was performed by Bechtel Co.. That effort consisted of borings and cone penetration test soundings for both the embankment and the foundation layers to depths of 150 ft below the surface. This latest extensive soil testing was prompted by a serious soil depression which appeared on the downstream embankment section. Field geophysical investigations were also made to determine the seepage conditions in the embankment. This effort included *in-situ* permeability testing as well as the installation of piezometers. The focus of the geophysical study was to identify possible piping (internal erosion) in the embankment that led to excess seepage and downstream ground subsidence.

Based on a review of the available documentation of the various site explorations, the soil profile and condition of the Par Pond Dam and its foundation can be characterized as follows:

**Embankment:**

The embankment consists of two primary zones and a downstream earth blanket. The latter was placed after the construction of the dam in order to help control excess seepage. The two primary zones are an *impervious* upstream zone making up about seventy percent of the embankment and a *pervious* downstream zone. Figure 2.1 depicts the cross section of the Par Pond Dam showing the two embankment zones.

The *impervious* zone consists of various types of sand with some subzones of silty clay. From the penetration resistance tests it has been established that the Corrected Standard Penetration Resistance, $N_{1-60}$, ranges between 12 and 25 blows per foot. This indicates that the upstream section of the embankment is firm. Other key soil properties that have been deduced from the various tests are the permeability of the section ranging from $3.9x10^{-6}$ to $2.8x10^{-4}$ feet per minute and the soil density which ranges from 114 to 117 $\frac{lbs}{ft^3}$ for dry soil. The cone penetration tests provided the

shear wave velocities which in turn enabled the evaluation of the soil shear moduli. Specifically, for the *impervious* section the shear wave velocities were found to be 1120 ft/sec and 1266 ft/sec for unsaturated and saturated soils respectively.

The *pervious* zone which constitutes the downstream part of the embankment consists primarily of sands with spots of coarse sand and gravel. From the Corrected Standard Penetration Test it has been assessed that a representative blow count for the section is greater than 50 blows per foot. The **field** permeability of the section ranged from $2.8x10^{-5}$ to $3.1x10^{-4}$ feet per minute. The *in-situ* dry density of the pervious section is 110 pcf. Since cone penetration tests were not made for the section, estimates of the shear wave velocity based on test could not be made. However, the shear wave velocities are safely assumed to be similar to those of the impervious section. Based on the Standard Penetration Test (SPT) it is expected that the pervious section should exhibit undrained strengths greater than those of the impervious section. Such a differentiation can only be attributed to the friction angle of the soil. Based on the test results and experience on similar soils, it was estimated that the friction angle in the impervious zone should be at least 32 degrees while for the pervious zone at least 35 degrees.

**Foundation Layers:**

The embankment foundation consists basically of two distinct layers over a firm base. The *upper* foundation layer is primarily sand and has a thickness of about 35 feet. Penetration test results for this layer showed blow count values ranging between 20 and 50 per foot. From the penetration resistance one can conclude that the layer consists of dense soils. The shear wave velocity for the layer has been estimated to be the same as that of the saturated impervious embankment section (1266 ft/sec). Similarly the soil density has been estimated to be the same as the density of the impervious section or 114 to 117 lbs/$ft^3$. From the SPT results the strength of the soil in the upper foundation layer is consistent with a soil having friction angle $\phi$ greater than 35 degrees.

The second layer is mostly poor sands and is approximately 70 feet thick. The SPT indicated that this layer consists primarily of weak spots exhibiting blow counts between 0 and 10 blows per foot. Sublayers of high penetration resistance are also present. The blow count within these stiff

spots is at places as high as 50 blows per foot. On the basis of the penetration resistance, this layer has been characterized as the *critical* layer with susceptibility to liquefaction. The soil density of this saturated layer is assumed to be the same as that of the upper foundation layer. From the test results it was determined that the shear wave velocity within the critical layer ranged from 300 to 1300 ft/sec. A median value of 770 ft/sec has been assigned to represent the layer as a uniform medium. The strength properties of this layer (cohesion and friction angle) are expected to be lower than those of the other zones. The undrained steady state strength, $S_{us}$, has been estimated to range between 0 and 500 pounds per square foot.

Figure 2.2 depicts the SPT results from the various boreholes and which helped to identify the different zones.

Figure 2.3 shows the permeability profile of the cross section which resulted from the geophysical exploration effort to determine the cause of the excess seepage.

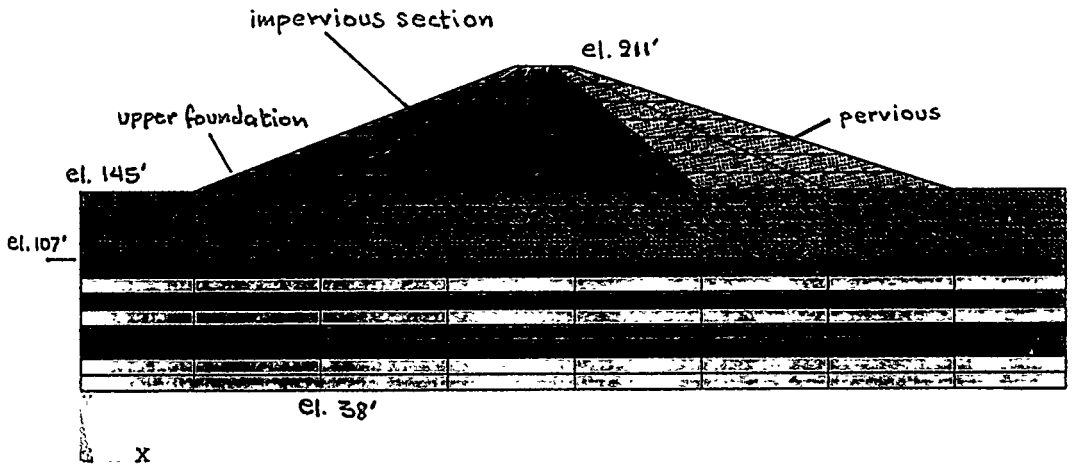


**Figure 2.1** Cross Section of Par Pond Dam and Foundation

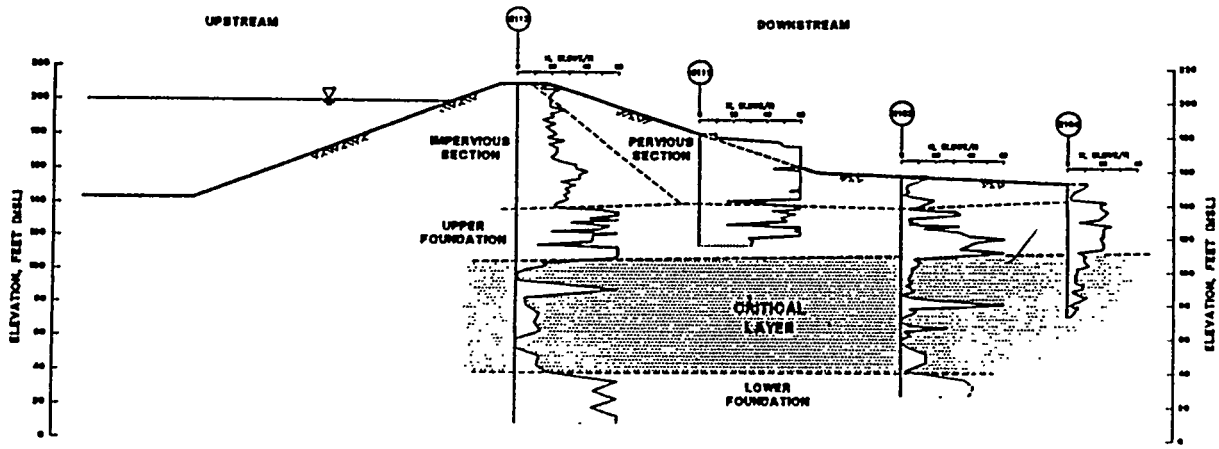


**Figure 2.2** Profile of the Standard Penetration Resistance

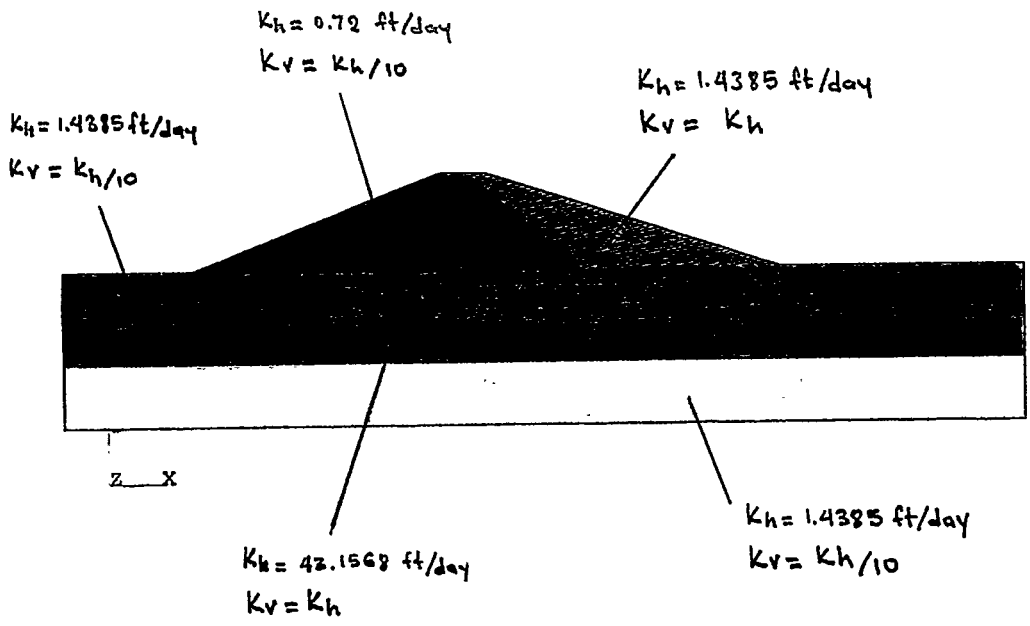


**Figure 2.3** Permeability Profile for Embankment and Foundation

# 3. REAME ANALYSIS

The adverse conditions that suddenly appeared in the Par Pond Dam prompted a number of analyses in order to identify (a) the possible cause of the degradation and (b) to assess the potential to failure. The presence of the critical layer below the embankment amplified the safety concerns especially when the response to postulated seismic excitations was considered. This *weak* foundation layer is more susceptible to liquefaction. Liquefaction in the layer, accompanied by loss of strength during an earthquake, can lead to large deformations or failure of the embankment. Consequently, not only slope failure due to insufficient structural integrity during a seismic event but also slope failure due to seismically induced liquefaction and their coupled effect must be considered. That is the seismic stability of the dam must be viewed via two failure modes, namely, (1) slope sliding in which failure is seen as a movement of a whole section of the embankment along a failure surface and (2) loss of strength due to liquefaction of the soil.

In order to obtain an initial assessment of the seismic stability of the dam, a quasi-static analysis was first used. This analysis provided a conservative estimate of the slope sliding potential under steady-state and dynamic conditions. Further, it provided a basis to evaluate other analyses performed for the same problem.

For the quasi-static evaluation of the stability of the Par Pond Dam BNL employed the commercially available REAME code.

## 3.1 Code Description

The REAME (Rotational Equilibrium Analysis of Multilayered Embankments) program is capable of determining the factor of safety against sliding failure of a slope based on a cylindrical failure surface and the simplified Bishop method, see Figure 3.1.1.

The program can handle (a) different soil zones, (b) seepage in the form of a specified piezometric surface, (c) excess pore pressure that can result during construction (in the form of a pore pressure ratio) and (d) identification of the most critical failure surface under given soil conditions.

It has the limitation that seismic loads can only be simulated with

a static equivalent (pseudo static method) and it cannot consider vertical seismic loads.

The theoretical basis of the REAME program is outlined in detail in Reference 1.

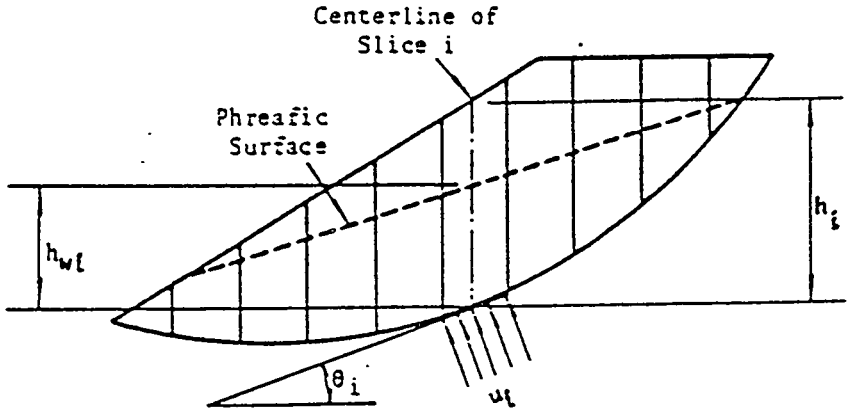


**Figure 3.1.1** Typical Dam Cross Section with a Failure Plane

Given a phreatic surface, the pore pressure

$$u_i = \gamma_w h_{w_i} \tag{3.1}$$

is calculated along its intersection with the failure surface ($\gamma_w$ is the unit weight of water).

The factor of safety against slope sliding is defined as the ratio of the resisting moment due to the shear resistance along the failure surface and the driving moment due to the weight and seismic force.

## 3.2 Par Pond Dam REAME Results

Shown again below is a cross section of the Par Pond Dam and the underlying foundation layers. Along with the geometry the figure also shows the variation of the standard penetration blow count. Four distinct regions in the cross section can be identified. The *critical* layer is the lower part of the foundation strata.

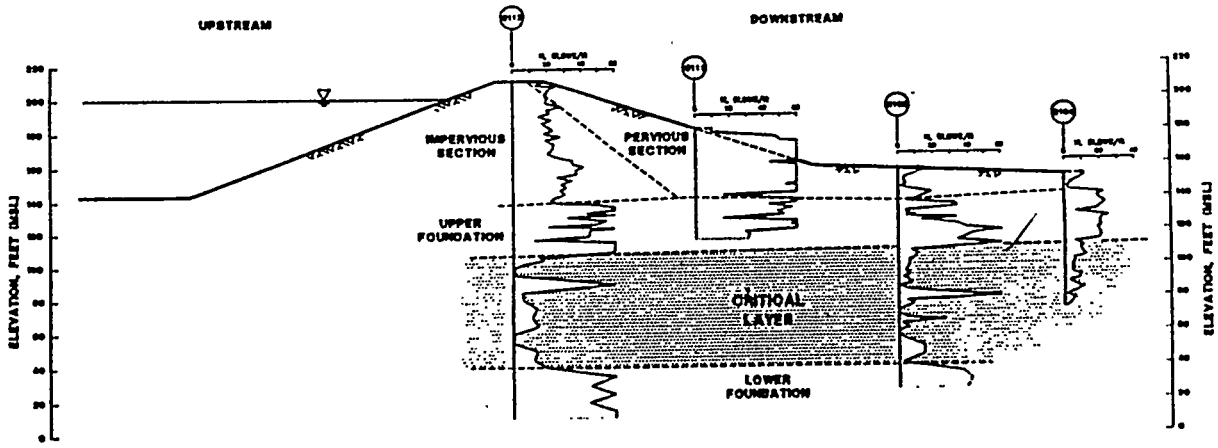


**Figure 3.2.1** Par Pond Dam Cross Section - SPR Profile

From the blow count data it is apparent that the embankment and the upper foundation layer are firm. It is also apparent that there are spots within the *critical* layer that must be very loose since they could not withstand any blows. Within that layer, however, there are sublayers that are quite stiff which in turn promote stability. By considering the critical layer to be uniform and with soil properties consistent with those of the weak spots, the resulting assessments should be overly conservative. Alternatively, one may assume an average soil behavior for the critical layer or subdivide the layer into appropriate weak and stiff sublayers.

A key to the stability analysis is to correlate the standard penetration resistance test results with soil friction angle $\phi$'s and values of cohesion **c** for the layers under consideration. Laboratory tests with similar soils have indicated that sands which can resist 6 blows per foot in standard penetration testing should exhibit friction angles of $30^o$ or better. Soils with smaller penetration resistance possess friction angles that could range between 30 and 0 deg. (zero representing the limiting case where the soil is completely loose and can take no shear).

In order to establish a basis for the evaluation, given the uncertainties in the soil properties that should be assigned to the critical layer, a whole spectrum of values for the friction angle and cohesion of the critical layer was considered. It was observed that the variation of the cohesion of the soil produced no significant effect in the calculated safety factors. Accordingly, the critical surfaces and the corresponding safety factors were calculated by varying the friction angle in the critical layer while maintaining its cohesion at a standard value. The upper foundation layer and the two embankment sections were assigned the friction angles specified in Chapter 2. The ultimate shear strength in the critical layer has been considered to be **Sus = 200 psf** which corresponds to cohesion **C = Sus/2 = 100 psf.**

For all sets of soil property values both the static and the equivalent seismic modes were analyzed with the REAME program. Figures 3.2.2-11 depict the variation of the safety factor against slope sliding with changes in the friction angle of the critical layer.

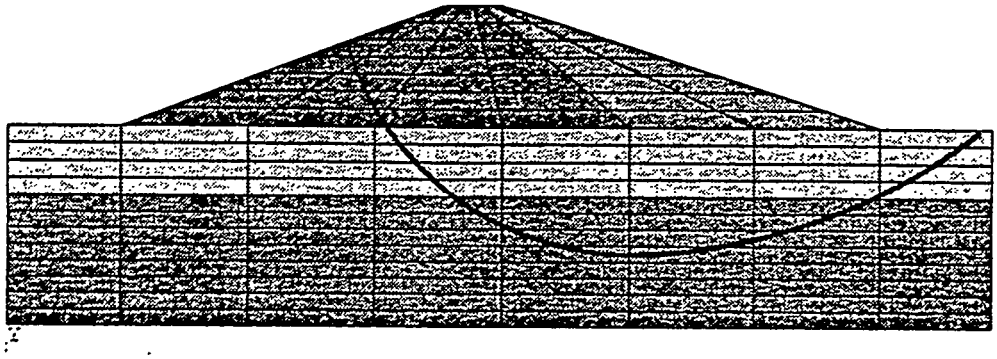

**Figure 3.2.2** Minimum Safety Factor and Location of Failure Surface under Static Conditions. **Friction angle** $= 3^o$, **Safety Factor = 0.262**

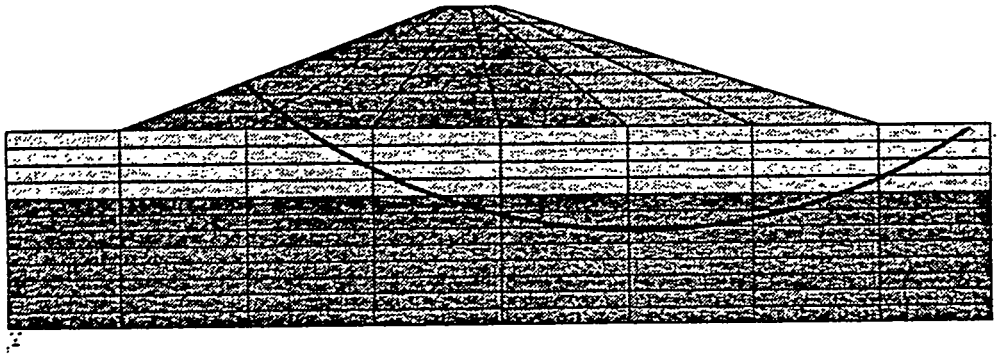

**Figure 3.2.3** Minimum Safety Factor and Location of Failure Surface in Seicmic Conditions. **Friction angle** $= 3^o$, **Safety Factor = 0.179.**

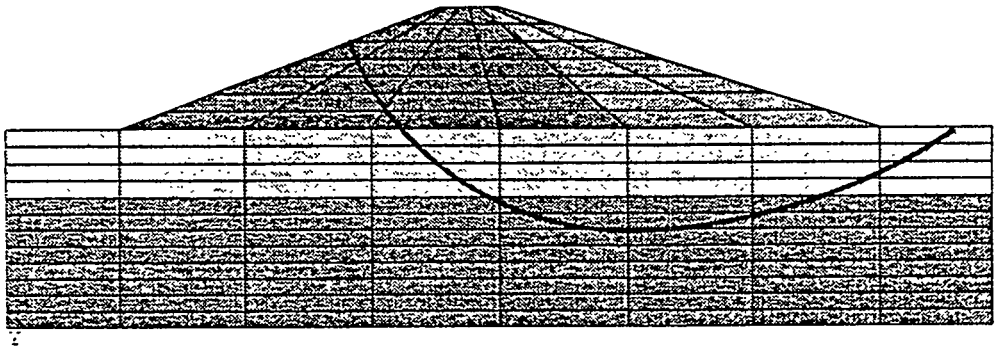

**Figure 3.2.4** Minimum Safety Factor and Location of Failure Surface under Static Conditions. **Friction angle** $= 6^o$, **Safety Factor = 0.417.**

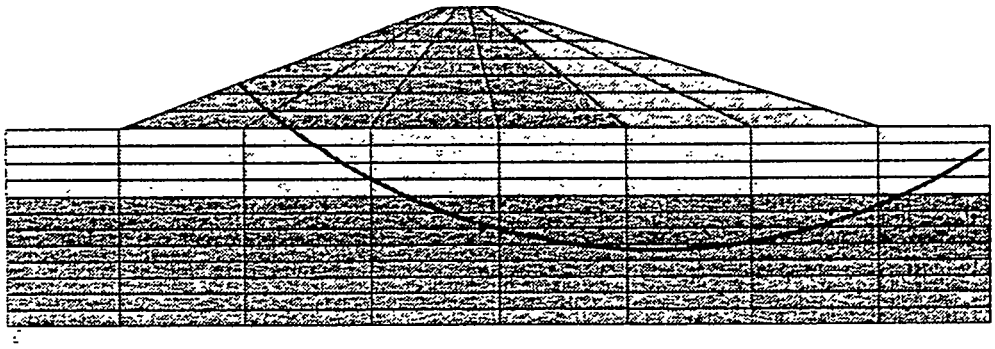

**Figure 3.2.5** Minimum Safety Factor and Location of Failure Surface in Seicmic Conditions. **Friction angle** $= 6^o$, **Safety Factor = 0.283.**

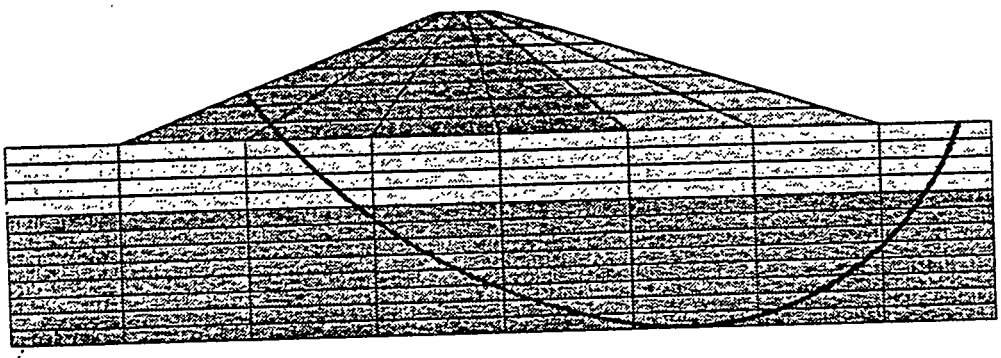

**Figure 3.2.6** Minimum Safety Factor and Location of Failure Surface under Static Conditions. $\phi = 12^o$, Safety Factor = 0.826.

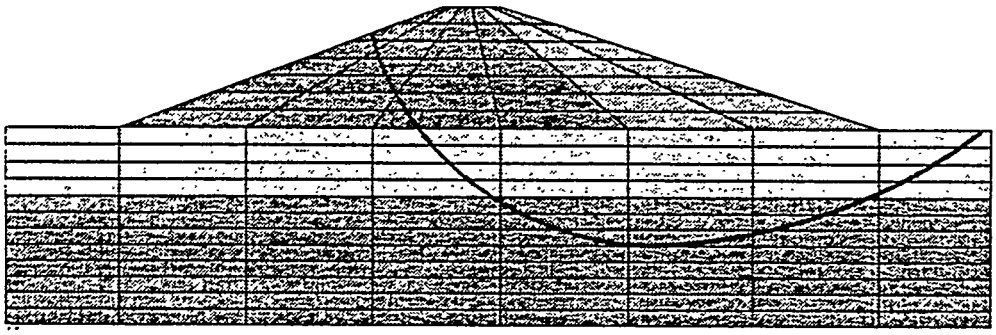

**Figure 3.2.7** Minimum Safety Factor and Location of Failure Surface in Seicmic Conditions (0.10 g). $\phi = 12^o$, Safety Factor = 0.535.

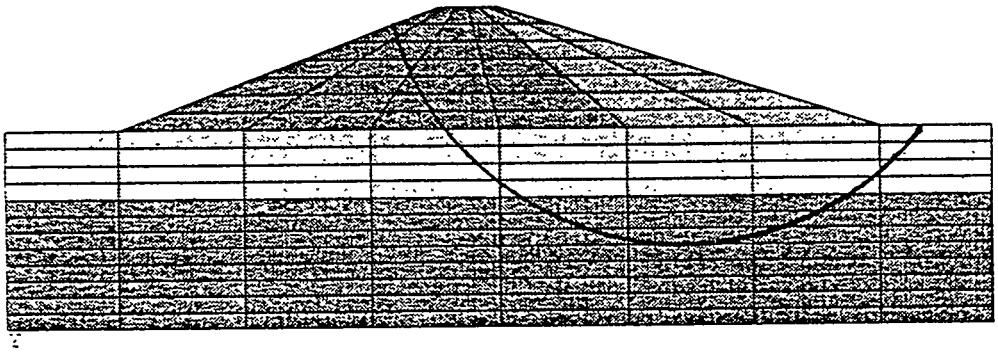

**Figure 3.2.8** Minimum Safety Factor and Location of Failure Surface under Static Conditions. $\phi = 24^o$, Safety Factor = 1.55.

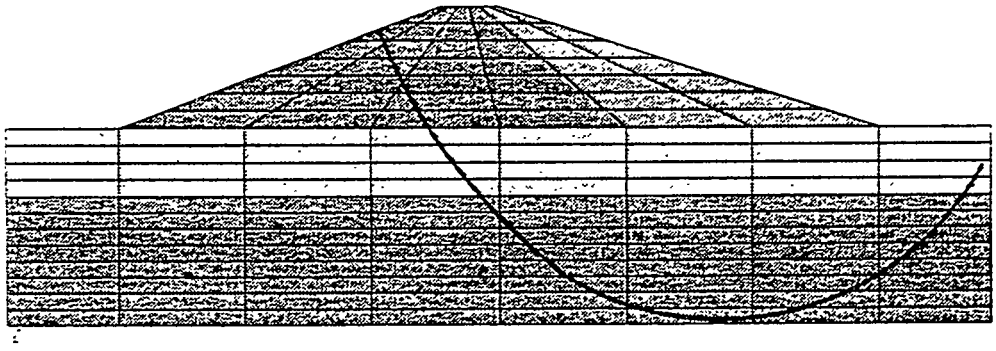

**Figure 3.2.9** Minimum Safety Factor and Location of Failure Surface in Seicmic Conditions (0.10 g). $\phi = 24^o$, Safety Factor = 0.985.

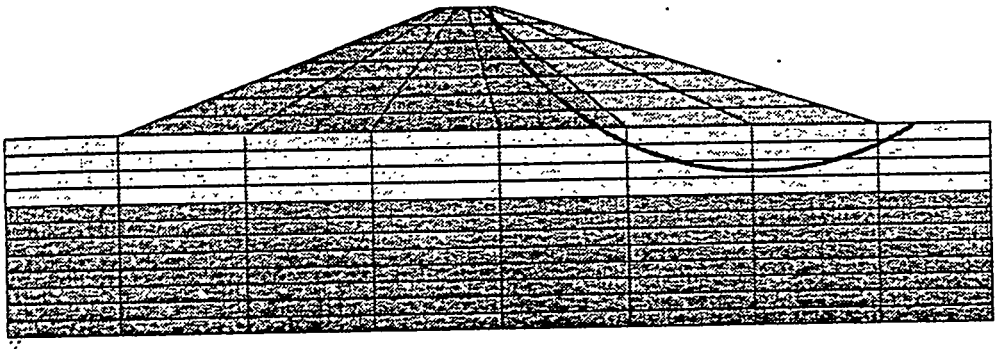

**Figure 3.2.10** Minimum Safety Factor and Location of Failure Surface under Static Conditions. $\phi = 30^o$, Safety Factor = 1.565.

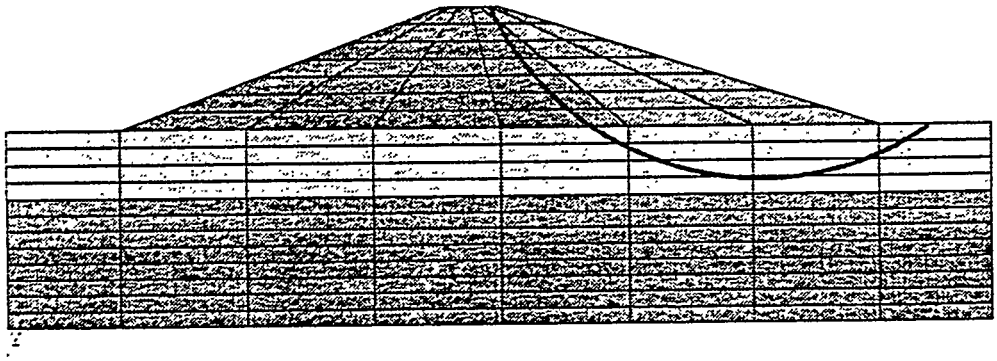

**Figure 3.2.11** Minimum Safety Factor and Location of Failure Surface in Seicmic Conditions (0.10 g). $\phi = 30^o$, Safety Factor = 1.20.

On the basis of these results the following observations can be made:

a. The critical surface, along which sliding of the mass above it can occur, shifts with changes in the frictional angle but always penetrates into the critical layer for friction angles less than $30^o$.

b. For friction angles in the critical layer less than $18^o$, the safety factor drops below 1.0 dipping to unacceptable values at friction angles less than 12 deg. (assessments (a) and (b) are for the static mode only).

c. With a seismic coefficient of 0.10 corresponding to a 0.10 g earthquake representative of the dam's location in the seismological map, the safety factors are reduced drastically. This strong reduction is consistent with the large degree of conservatism associated with the seismic coefficient. For a more realistic assessment of the seismic stability an actual earthquake record more representative for the site, should be used.

d. If values for the frictional angle in the weak layer are to be deduced based on this analysis, considering that the dam is intact under static loads, it is reasonable to say that an equivalent value $\phi = 12$ deg. should conservatively be considered as the lowest bound. The analysis calculated a value of $\mathbf{SF = 0.826}$ for static loads and $\phi = 12$ deg., which is lower than the desirable safety factor limit of 1.0. Given the uncertainties and conservatism inherent in the analysis, a safety factor just below 1.0 does not necessarily indicate an immediate failure.

e. A discretization of the critical layer into weak and stiff sublayers led to higher safety factors.

f. No explicit relation between the penetration resistance and the frictional angle $\phi$ exists. Given that the analysis results are acutely sensitive to the specific values of $\phi$ further soil testing to define the $\phi$ profile in the critical layer is recommended if more accurate determinations of the dam integrity are to be made.

g. The construction of a downstream berm as a corrective action appears to have merit since it increases the safety factor and shifts the location of the potential failure surface. This assessment, however, should be considered very preliminary. First it must be realized that failure as a result of slope sliding can happen anywhere on the dam. If the condition of the soil in the critical layer is so poor that the only remedial

action is the construction of a berm, the likelihood of upstream sliding failure must also be considered. For this the berm will be of no benefit.

Use of the REAME program provided some insight of the potential for slope failure, including the possible locations of failure. However, it lacked the sophistication needed to incorporate a realistic earthquake excitation or to consider vertical earthquake loads. Further, the program cannot be used to address the liquefaction question. Since liquefaction under the action of seismic loads can be very damaging, the limitation of the program is critical. Given the limitations, the REAME evaluations must be viewed as the preliminary first step to be augmented with more sophisticated evaluations.

# 4. EVALUATION OF FAILURE POTENTIALS

The evaluation of the failure potential of the Par Pond Dam is performed through a series of analyses each of which addresses a specific aspect of the stability problem. With the various analyses the seepage forces, the steady state stress conditions, the earthquake induced stresses, the potential to slope failure and the potential to liquefaction are evaluated. As it will be seen in the following analysis, the information deduced from the different steps will eventually converge in order for a comprehensive assessment of stability to be made.

## 4.1 Seepage Analysis

The seepage analysis of the Par Pond Dam represents the first element of the detailed evaluation of dam safety.

Specifically, this step provides the distribution of the pore water pressure in the embankment and its foundation. The pore pressure distribution will be used to calculate the steady-state effective stress in the soil. The effective stress constitutes a key parameter in the safety analysis, especially in the evaluation of the liquefaction potential.

The seepage analysis can also be used to resolve questions regarding the present condition of the soil in the embankment and the foundation layers. On the basis of comparisons between the observed and the calculated amount of seepage through the dam and foundation the current permeability properties of the soil can be established and then compared to the permeability values that the soil possessed when the dam was constructed.

To solve the seepage problem the ANSYS general purpose program is utilized. This program enables the solution of the heat equation (which is also the model equation for the seepage problem) in a finite element analysis scheme.

Figure 4.1.1 depicts the soil permeability profile of the dam cross section implemented in the BNL seepage analysis.

The governing equation of **steady unconfined seepage** can be seen in the form,

$$k_x \frac{\vartheta h(x,y)}{\vartheta x^2} + k_y \frac{\vartheta h(x,y)}{\vartheta y^2} = 0 \qquad (4.1.1)$$

where, $h(x,y)$ = total head and $k_x, k_y$ = soil permeabilities.

The pore pressure is deduced from the total head distribution according to the relation,

$$p_f = h - y \tag{4.1.2}$$

where $p_f, y$ are the pore pressure and the vertical elevation respectively.

The term *unconfined* refers to the undefined location of the phreatic surface. The phreatic surface represents the boundary across which there is no flow of water in the normal direction, $\dot{q}_n = 0$, and the pore pressure is zero $p_f = 0$. Figure 4.1.2 depicts the boundary conditions that are applicable to the problem at hand. The system variable **h(x,y)** represents the total head and it is the sum of the elevation head (with respect to an reference elevation) and the pressure head. Figure 4.1.3 shows the finite element discretization of the domain.

The location of the phreatic surface is determined through an iterative procedure that minimizes the difference between the total head and the elevation head over an assumed phreatic surface. After an initial assumption on the location, the surface location is varied until the criterion is satisfied. The boundary conditions on the rest of the system remain unchanged during that process. Specifically, the part of the boundary that is wetted by the reservoir is assigned a total head equal to the pool level elevation in its entirety, i.e.

$$h(x,y) = y(x,y) + \gamma_w d = H \qquad \text{(H = pool elevation)}$$

Upon solution of the problem, the total head, shown graphically in Figure 4.1.4, and the flow velocity field, Figure 4.1.5, become available. In the solution process, the effect of changes in the permeability on the pore pressure field (that implies changes in the location of the phreatic surface) were also studied. This was done to account for uncertainties in the permeability values. It was found that changes in the pore pressure in the critical zone of the foundation strata are only slightly effected by the changes in the permeability.

Lastly, the changes in the flow and total head fields caused by a soil blanket or a berm on the downstream face of the dam were assessed. Figure 4.1.6 depicts two downstream berm structures while the resulting pore pressure distribution and seepage are shown in Figure 4.1.7.

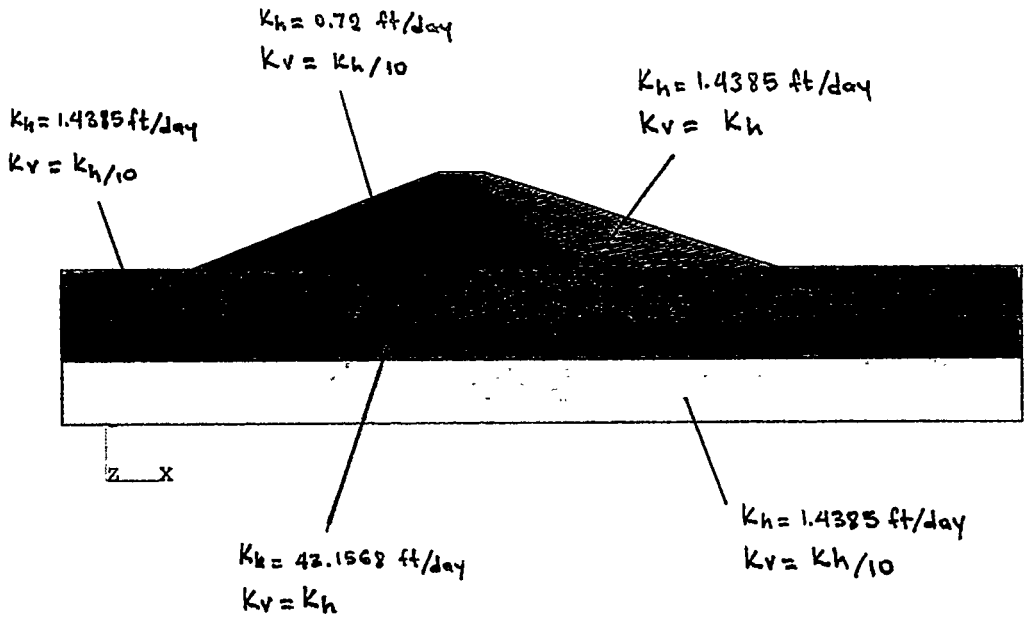


**Figure 4.1.1 Soil Permeability Profile**

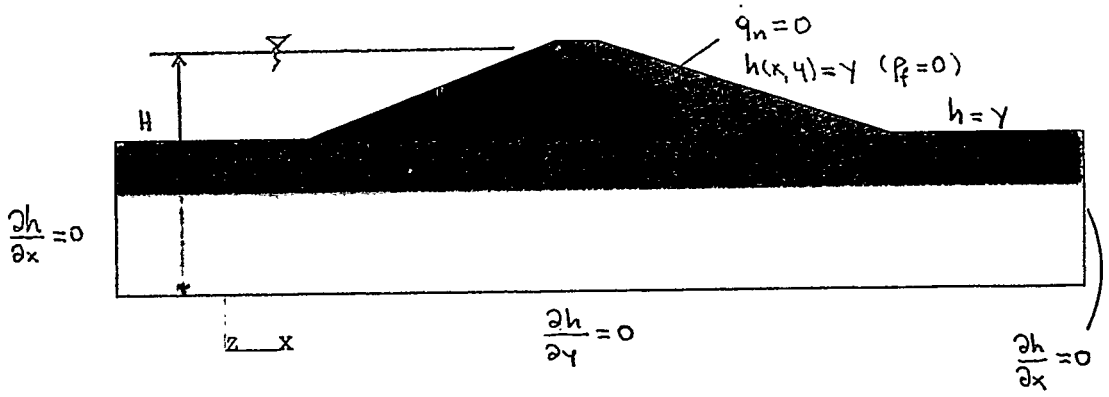


**Figure 4.1.2 Boundary Conditions of the Seepage Problem**

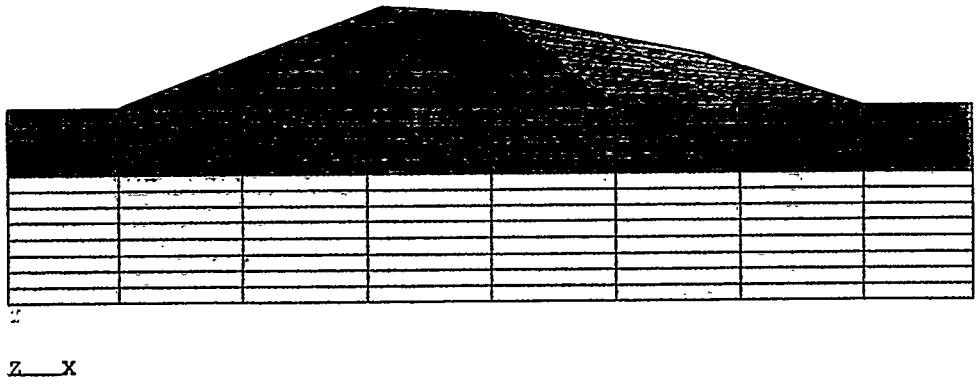


**Figure 4.1.3 Finite Element Discretization of Seepage Problem**

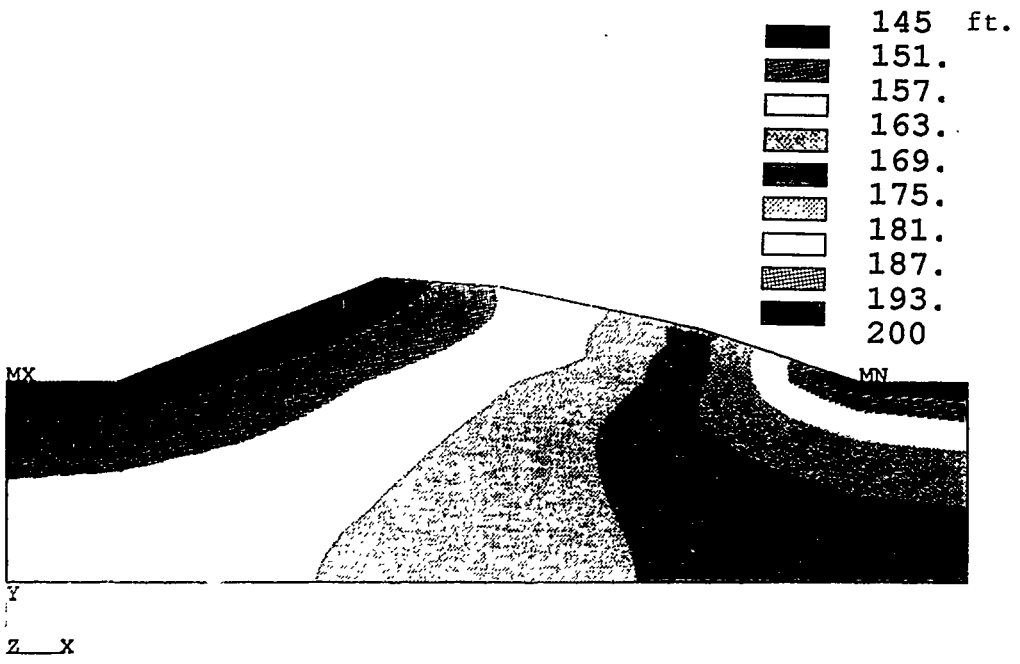


**Figure 4.1.4 Total Head Profile**

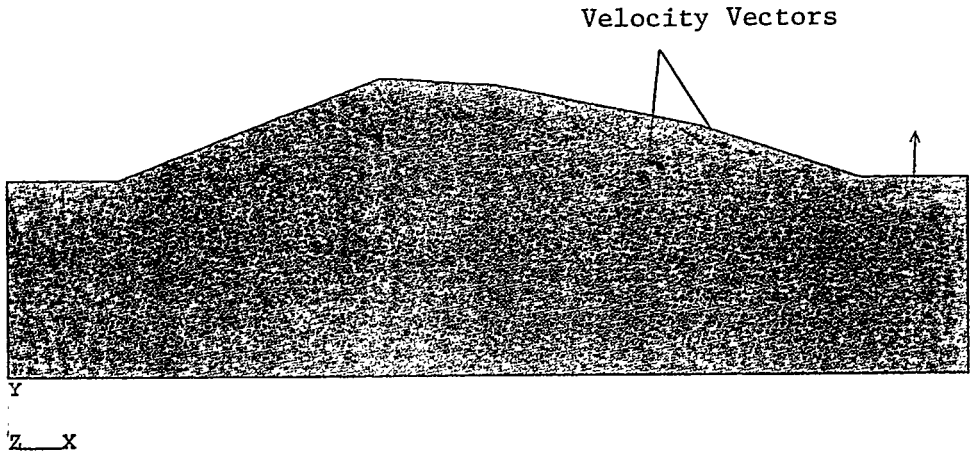


**Figure 4.1.5 Seepage Flow Velocity Distribution**

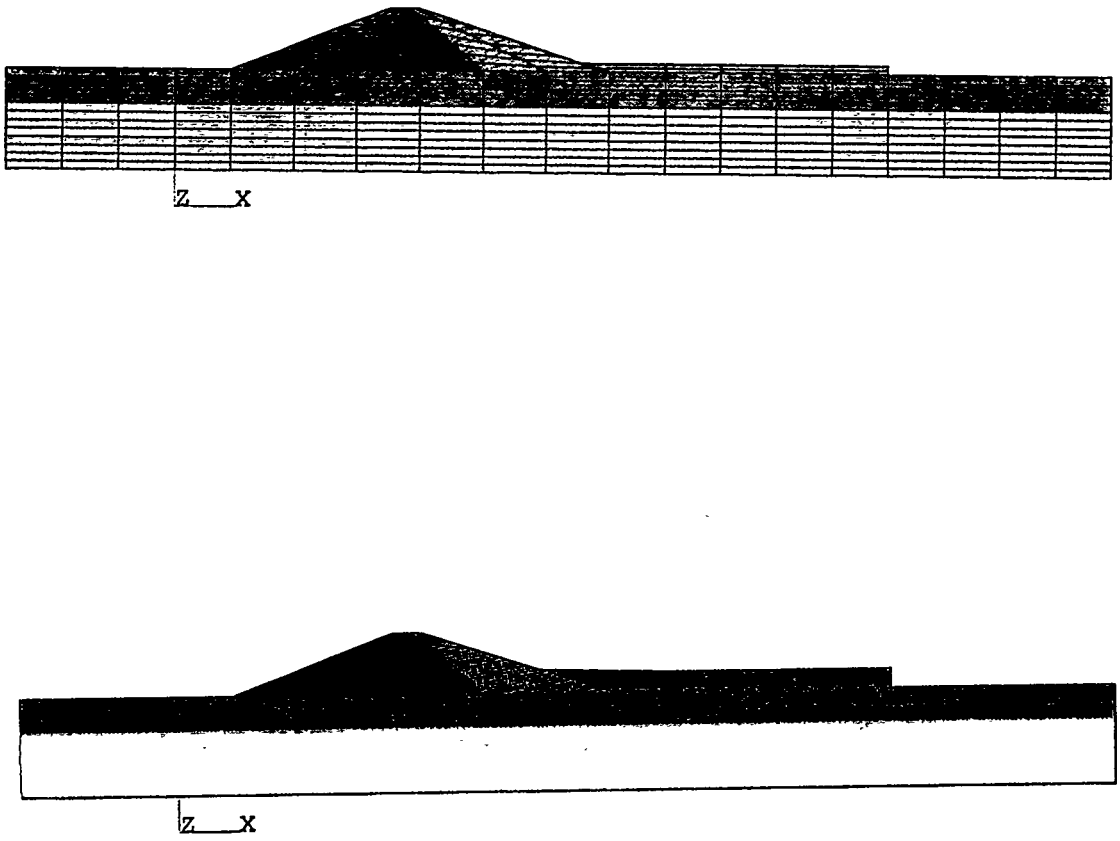


**Figure 4.1.6 Dam models incorporating a downstream berm.**

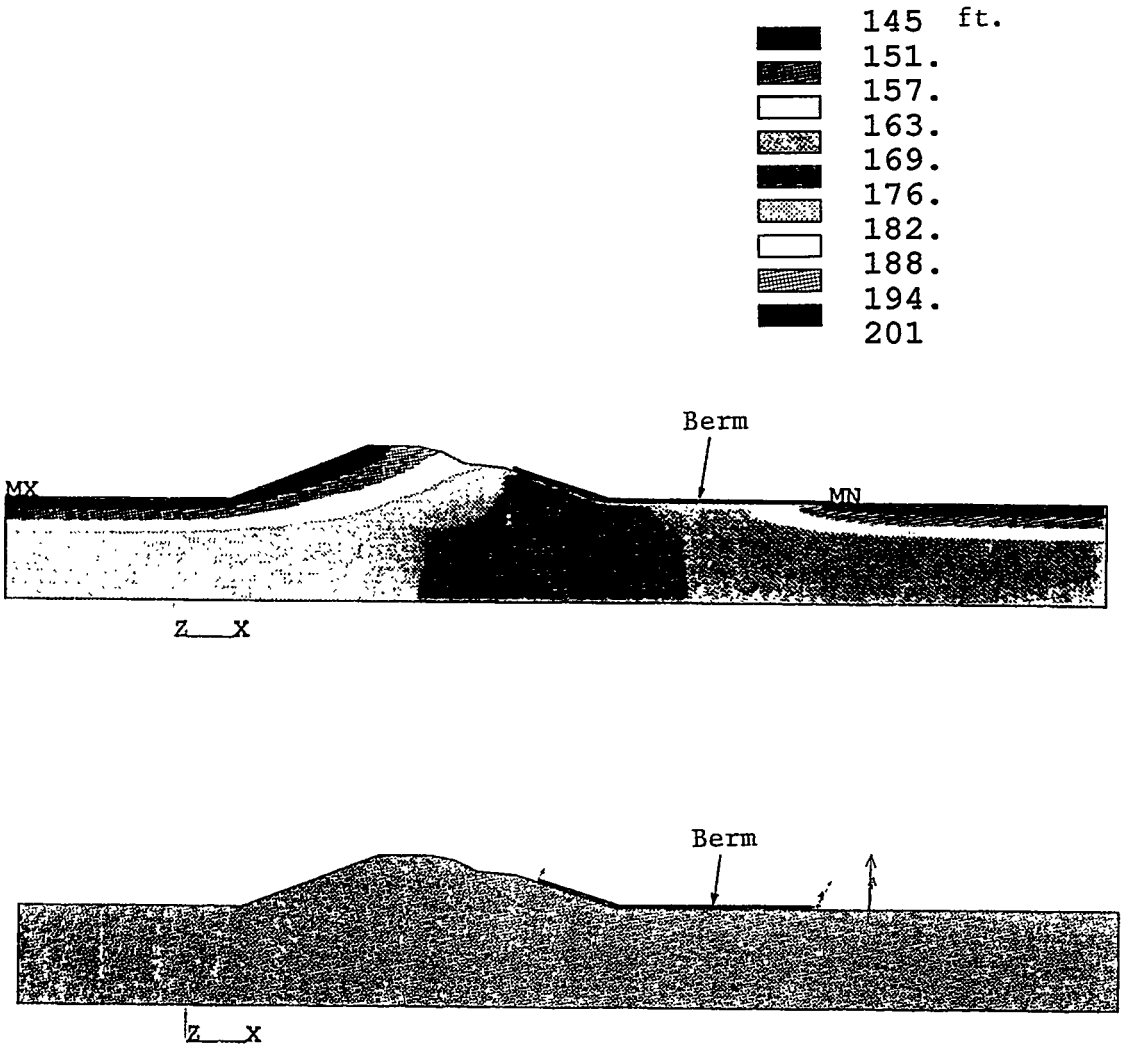


**Figure 4.1.7 Total Head and Velocity profile resulting from berm structures.**

## 4.2 Steady-State Stress Conditions in Embankment and Foundation

The stress field prior to a seismic event in the embankment and the foundation layers constitutes an important element in the stability integrity evaluation. The static stress conditions are key components in the definition of the factor of safety against slope failure. Further, the overburden initial stress is vital information to a liquefaction potential analysis because of its relation with the effective stress that controls the process of liquefaction. It should also be mentioned that the initial shear stress field has been the focus of a number of investigative works as an influential mechanism in the liquefaction process. Thus, it is of utmost importance for the analysis to obtain a good description of the initial stress field.

Elastic properties, such as shear modulus and Poisson's ratio, are deduced from test field data (obtained by GEI Consultants Inc.) on shear wave velocities. Soil unit weights have also been assessed.

The stress field in the system is the result of the soil overburden and of the weight of the water in the reservoir. The analysis utilized the ANSYS program for the finite element solution. The cross section of the dam and foundation is considered to be under a plane strain state of stress (due to the width of the embankment).

The discretization process identified the different zones of material as shown in Figure 4.2.1. A variation of the model shown in Figure 4.2.1 was also used, see Figure 4.2.2, in which the critical layer of the foundation was further discretized into weak and stiff sublayers. Additional models that incorporate a berm extension of the downstream face of the embankment have also been studied to address the influence of such structure on the liquefaction potential in the critical zone.

The finite element solution indicates that, as expected, the overburden stress is maximum at the bottom of the critical zone and directly below the embankment reaching values of 20,000 psf, see Fig.4.2.4. The shear stresses are higher in the downstream face and specifically at the intersection of the

embankment and the foundation, Figures 4.2.5,6. High static shear stress values are seen directly below the downstream face at the bottom of the critical zone (see Figures 4.2.5-6). Also shown are the total stresses $(\sigma_{xx}, \sigma_{yy})$. The shown stresses result from the combined loads of soil overburden and the reservoir weight.

Upon evaluation of the static stress field, the critical parameter of the effective overburden stress $\sigma_0$ is deduced from the relation,

$$\sigma_0 = \sigma_{yy} - \alpha p_f \tag{4.2.1}$$

where $\sigma_{yy}$ is the overburden stress and $\alpha$ is the compressibility of the soil fraction ($\alpha = 1.0$ in this analysis).

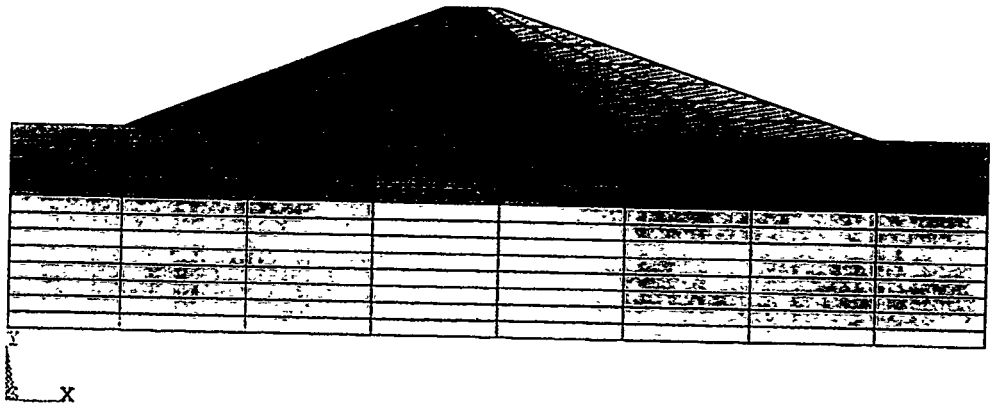


**Figure 4.2.1 F.E. Descritization with Uniform Critical Layer**

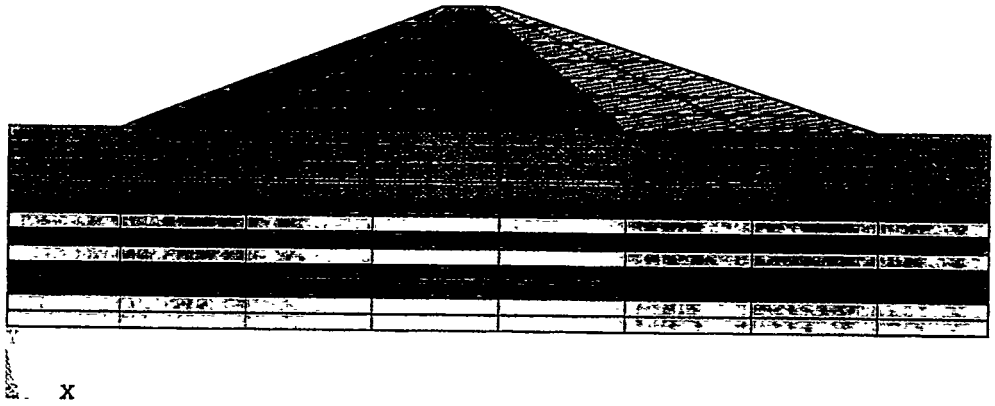


**Figure 4.2.2 F.E. Model with Non-Uniform Critical Layer**

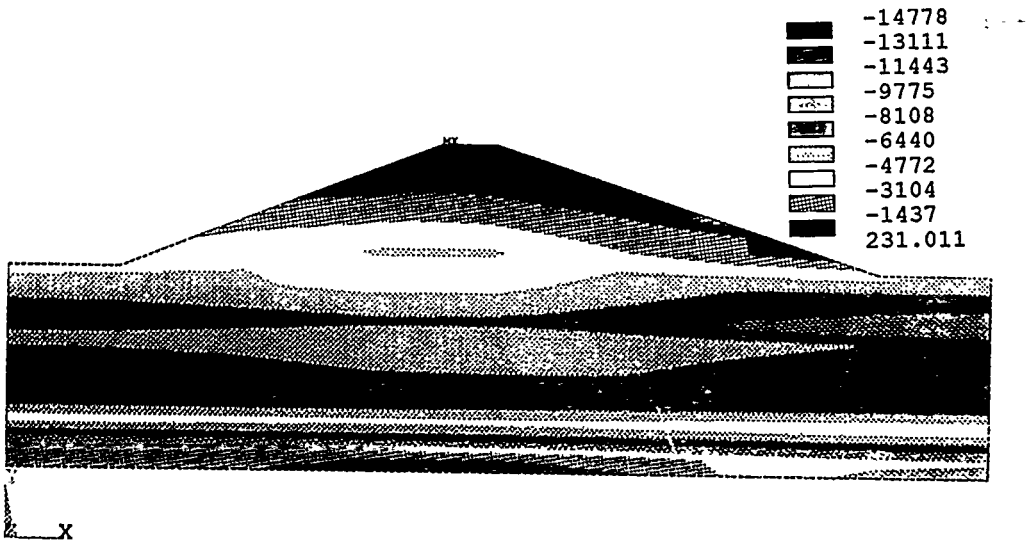


**Figure 4.2.3 Horizontal ($\sigma_{xx}$) Steady State Stresses**


**Figure 4.2.4 Vertical ($\sigma_{yy}$) Steady State Stresses**

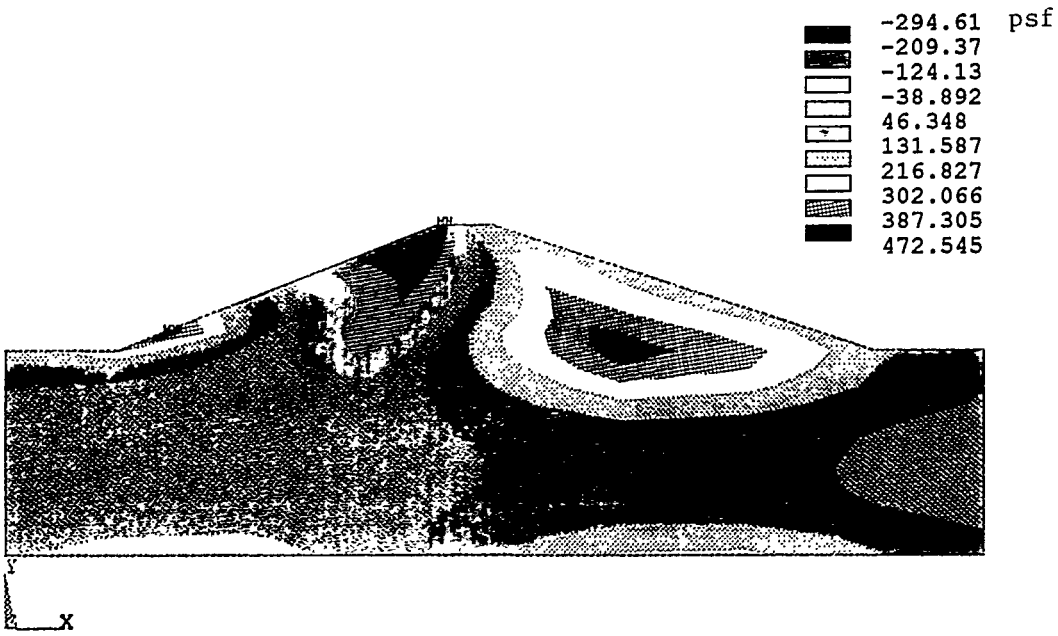


**Figure 4.2.5 Shear ($\tau_{xy}$) Steady State Stresses (model A)**

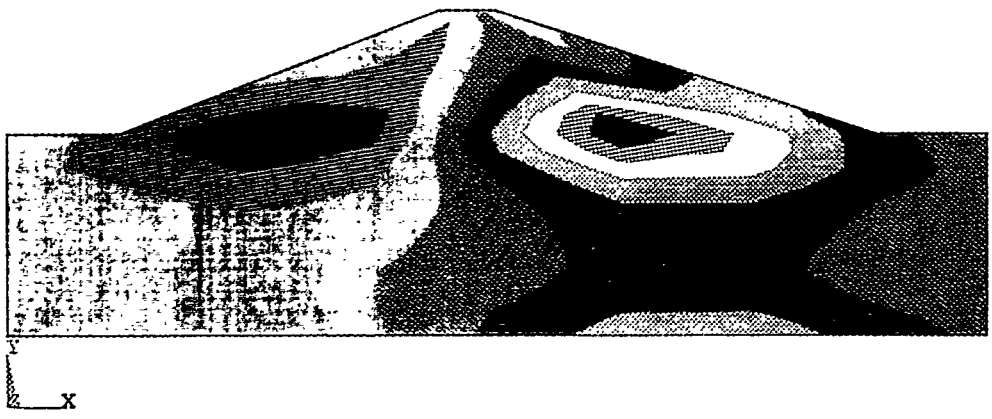


**Figure 4.2.6 Shear ($\tau_{xy}$) Steady State Stresses (model B)**

## 4.3 POROSLAM Earthquake Analysis

The need for an analysis that would use an earthquake event appropriate for the site and treat the medium in a more sophisticated manner, has been discussed earlier.

The mechanism of slope failure can be viewed as a critical state of stress within the embankment. Thus, the response of the dam to an actual earthquake and the variation of the state of stress during such event is an important element in determining its integrity. The fact that the medium is (at least part of it) saturated with water influences the way the dam cross section will respond to an earthquake event. The pore pressure of the water trapped in the soil skeleton will fluctuate as the earthquake waves come through and affect the intergranular soil stresses. Since the strength of the soil is affected by the intergrannular stresses, it is vital that the dynamic pore pressure be captured. To simulate the coupled behavior of pore water and soil skeleton requires treating the medium as a two-phase system with governing equations established appropriately.

The ability of the soil to resist liquefaction is dependent on both its initial stress state (effective stress) and on the the intensity of the dynamic shear stresses. The shear stress variation at different locations in the embankment and the foundation and especially the number of stress cycles (and their intensities) during the earthquake event determine whether the soil is susceptible to such failure.

Thus, the theoretical/computational model used must allow;

a. representation of the domain as a two-phase medium

b. consideration of actual or representative earthquake inputs

c. consideration of the time history record of the dynamic stresses caused by the seismic excitation as an input

In order to satisfy the above criteria, the POROSLAM program was used. This finite element code has been developed at the Earthquake Center of the City University of New York.

**Program Description:**

The POROSLAM program uses a two-dimensional finite element representation of Biot's dynamic equations for both soil and fluid phases. Biot's equations are a description of the response of the soil skeleton and the pore water. The formulation is based on the linear form of the governing equations, making the analysis linear. Nonlinear soil behavior is compensated for with the consideration of hysteretic soil damping.

The governing equations reflecting the dynamic behavior of an infinitesimal soil element are,

$$\frac{\vartheta \tau_{xx}}{\vartheta x} + \frac{\vartheta \tau_{xy}}{\vartheta y} = \varrho \ddot{u}_x + \varrho_f \ddot{w}_x$$

$$\frac{\vartheta \tau_{yx}}{\vartheta x} + \frac{\vartheta \tau_{yy}}{\vartheta y} = \varrho \ddot{u}_y + \varrho_f \ddot{w}_y$$

and

$$-\frac{\vartheta p_f}{\vartheta x} = \varrho_f \ddot{u}_x + \frac{1}{f}\varrho_f \ddot{w}_x + \frac{\eta}{k}\dot{w}_x$$

$$-\frac{\vartheta p_f}{\vartheta y} = \varrho_f \ddot{u}_y + \frac{1}{f}\varrho_f \ddot{w}_y + \frac{\eta}{k}\dot{w}_y \qquad (4.3.1)$$

where,

$[u_x, u_y]$ = components of soil displacement

$[w_x, w_y]$ = components of pore water displacement

$$\{\tau\} = (\tau_{xx}, \tau_{yy}, \tau_{xy})^T = \{\sigma_{xx} - \alpha p_f, \sigma_{yy} - \alpha p_f, \sigma_{xy}\}^T$$

while, $f$ = porosity, $\varrho$ = total mass density, $\varrho_f$ = fluid mass density, $\alpha$ = compressibility of the solid, $M$ = compressibility of the fluid, $\eta$ = fluid viscosity, and $k$ = soil permeability.

The resultant equation that expresses the total stress vector in terms of the displacement vector, with hysteretic damping considered, takes the form

$$\{\tau\} = E_c[D_0][D_1]\{u_x, u_y\}^T + E_c[D_3][D_1]\frac{\vartheta}{\vartheta t}\{u_x, u_y\}^T +$$

$$\alpha^2 M[D_2]\{u_x, u_y\}^T + \alpha M[D_2]\{w_x, w_y\}^T \qquad (4.3.2)$$

where,

$$[D_0] = \begin{bmatrix} 1 & \frac{\nu}{1-\nu} & 0 \\ \frac{\nu}{1-\nu} & 1 & 0 \\ 0 & 0 & \frac{1-2\nu}{2(1-\nu)} \end{bmatrix} \qquad [D_3] = \begin{bmatrix} \lambda_c & \frac{\lambda_c \nu}{1-\nu} & 0 \\ \frac{\lambda_c \nu}{1-\nu} & \lambda_c & 0 \\ 0 & 0 & \frac{\lambda_s(1-2\nu)}{2(1-\nu)} \end{bmatrix}$$

$$[D_1] = \begin{bmatrix} \frac{\vartheta}{\vartheta x} & 0 \\ 0 & \frac{\vartheta}{\vartheta y} \\ \frac{\vartheta}{\vartheta y} & \frac{\vartheta}{\vartheta x} \end{bmatrix} \qquad [D_2] = \begin{bmatrix} \frac{\vartheta}{\vartheta x} & \frac{\vartheta}{\vartheta y} \\ \frac{\vartheta}{\vartheta x} & \frac{\vartheta}{\vartheta y} \\ 0 & 0 \end{bmatrix}$$

$$p_f = -\alpha M(e_{xx} + e_{yy}) - M(\frac{\vartheta w_x}{\vartheta x} + \frac{\vartheta w_y}{\vartheta y})$$

$\lambda_c$ is the hysteretic damping ratio associated with hydrostatic compression while $\lambda_s$ represents the damping ratio associated with shear strains and $E_c = \frac{(1-\nu)E}{(1+\nu)(1-2\nu)}$.

The solution of the discretized equations is performed in the frequency domain. Thus the input, which represents the ground acceleration time history for a particular seismic event, is expressed in terms of its Fourier components and applied as a forcing function on the model. The ability of the program to develop Harmonic Unit Response solutions for the dam, allows a number of generated earthquakes to be studied. Such earthquakes could be described in the form of a response spectrum or a power spectrum. This feature is especially valuable in a probabilistic evaluation of the response for the domain under study.

Figure 4.3.1 outlines the overall problem of the embankment and its foundation from the dynamic standpoint. It also depicts the finite element discretization of the cross section used in the POROSLAM analysis which is the same as the one used in the static stress evaluation (Model A or Model B).

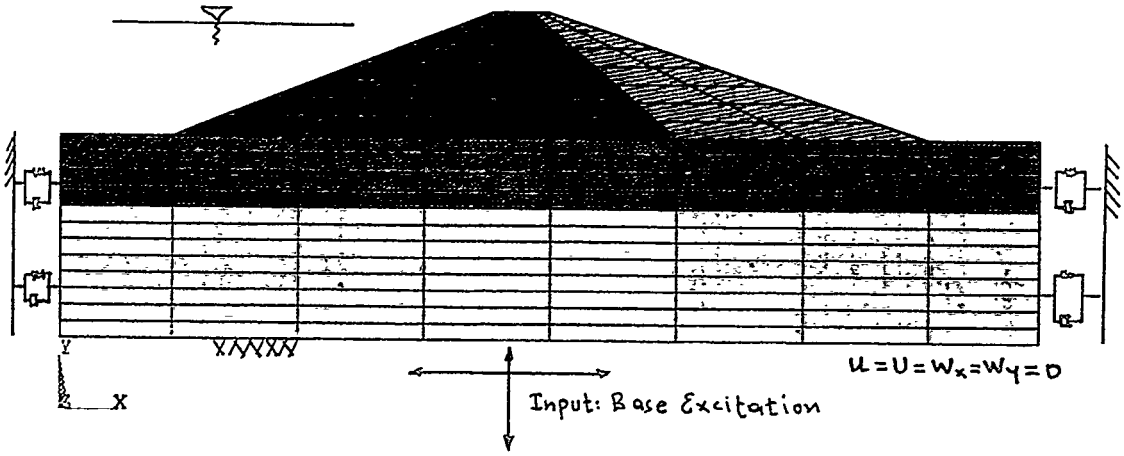


**Figure 4.3.1 Dynamic Problem Description of Par Pond Dam**

## Transmitting Boundaries

Implementation of transmmiting boundaries on the two sides of the model allowed for the propagation of waves outward. The transmmiting boundaries in the POROSLAM program simulate the continuation of both intergrannular stresses and pore pressures in the saturated soil (transmission in dry soil has been extensively used in a number of codes). The propagation is based on the 1-D wave equations of saturated soils where,

$$\tau_{xx} = E_c\left(\frac{\vartheta u_x}{\vartheta x} + \lambda_c \frac{\vartheta}{\vartheta t}\frac{\vartheta u_x}{\vartheta x}\right) + \alpha^2 M \frac{\vartheta u_x}{\vartheta x} + \alpha M \frac{\vartheta w_x}{\vartheta x}$$

$$p_f = -\alpha M \frac{\vartheta u_x}{\vartheta x} - M \frac{\vartheta w_x}{\vartheta x} \tag{4.3.3}$$

When transmission in the vertical direction at the bottom of the model is considered, the same relations are applicable ($\sigma_{xx} \rightarrow \sigma_{yy}$).

Shear transmission is also considered where transmission is achieved by continuation of the shear stresses along the boundary,

$$\tau_{xy} = \varrho V_s \dot{u}_s \tag{4.3.4}$$

where $\dot{u}_s$ = velocity in the direction of shear and $V_s$ = shear wave velocity of the soil.

The validity of the program has been successfully tested against established codes. In particular, the static mode for stresses and displacements has been checked with results obtained by the ANSYS code while the dynamic mode, in the form of base acceleration amplification, with the FLUSH code. These comparisons were performed for dry soil rather than saturated due to the inability of ANSYS and FLUSH to treat the soil as saturated medium.

## PAR POND DAM Finite Element Model

The dynamic response of the Par Pond Dam was evaluated using the finite element descritizations used in the steady state stress analysis (model A and model B). The soil properties assigned to the section and the earthquake excitation of the system are discussed in detail below:

### Soil Properties

The soil properties that influence the dynamic response of the dam are the shear modulus **G** the Poisson's ratio $\nu$, the unit weight $\gamma$ and the hysteretic damping $\lambda$.

From the GEI report (Ref. 6) of *in-situ* test data of unit weight and shear wave velocities as well as standard penetration resistance results in blows/foot, a profile of the important properties was deduced. Other unmeasured soil properties that enter the dynamic governing equations were assigned values that apply to similar soils.

The shear modulus is determined from the relation,

$$G = \rho V_s^2 \tag{4.3.5}$$

where,

$\rho$ = soil density (unit weight/32.2)

$V_s$ = shear wave velocity (ft/sec)

The specific values of the soil properties in the different zones of the embankment and the foundation layers are listed below

**critical layer**

For the uniform critical layer (model A) the soil properties assigned were,

$\gamma = 120$ pcf

$V_s = 800$ ft/sec

$\nu = 0.33$

$G = 2.38$ x $10^6$ psf

In an effort to correlate shear wave velocity measurements and standard penetration blow count for the critical layer, the Seed and Idriss approach was also used to estimate the shear modulus **G**.

From the static analysis coupled with the seepage analysis the *effective* overburden stress $\sigma_0^{'}$ was evaluated. From the effective overburden-blow count-relative soil density relationship the relative density of the weak layer was determined to range between

$$D_r = 20\% - 40\%$$

According to the Seed and Idriss formulation, the modulus for sand is likely to be of the order

$$G = 1.0 \cdot 10^5 \cdot \sigma_0^{'\,1/3} psf \quad .... \quad for \quad D_r = 0\%$$

$$G = 2.0 \cdot 10^5 \cdot \sigma_0^{'\,1/3} psf \quad .... \quad for \quad D_r = 100\%$$

The effective stress $\sigma_0^{'}$ ranges between 8 ksf and 5 ksf (higher at bottom) along the centerline of the dam. Interpolation of the relations for **G** above led to

$$G = 2.4 \cdot 10^6 \quad psf$$

which is remarkably close to the value determined from the shear wave velocity.

For a non-uniform critical layer, (Model-B), the soft layers are assigned the properties listed above while the stiff sublayers were assigned the values

$\gamma = 130$ pcf

$V_s = 1{,}200$ ft/sec

$\nu = 0.25$

$G = 5.814 \text{ x } 10^6$ psf

**foundation layer**

$\gamma = 130$ pcf

$V_s = 1{,}200$ ft/sec

$\nu = 0.25$

$G = 5.814 \text{ x } 10^6$ psf

**embankment**

- *saturated section* (below phreatic line)

$\gamma = 130$ pcf

$V_s = 1{,}200$ ft/sec

$\nu = 0.25$

$G = 5.814 \text{ x } 10^6$ psf

- *dry section* (above phreatic line)

  $\gamma = 130$ pcf

  $V_s = 1{,}100$ ft/sec

  $\nu = 0.25$

  $G = 4.88 \text{ x } 10^6$ psf

The uncertainties in soil damping for the site were addressed by analyzing the system for different damping levels. Damping ratios of **0.5 %**, **1.0 %** and **2.0 %** were introduced and the response of the dam for each was evaluated. It should be mentioned that **0.5 %** damping is very conservative while **2.0 %** is still conservative but more representative for the type of soil in the embankment and the foundation. Based on the dynamic analysis for the **0.5 %** damping, the effective strains in the critical layer were estimated to be **.13 %**. For such value of effective strain and for the soil type under consideration the corresponding actual hysteretic damping is in excess of **10 %**. Thus, the hysteretic soil damping of **2%** used in the analysis is conservative.

## Seismic Input

The definition of an earthquake input that is representative of the geographical location of the structure is key to the seismic analysis. Over the years, various families of earthquakes (represented by their response spectra) have been used for seismic analyses associated with the Savannah River complex. It should be expected that the response of the systems be different for the different earthquakes (even of the same peak acceleration).

Based on the latest consensus regarding the appropriate seismic excitation for the site, the input earthquake is chosen to be a **Charleston-like** event of intensity 0.11g (7.5 Richter scale and 20 sec strong motion). Specifically, the earthquake represents a ground motion that results from the attenuation of what is taken to be a Charleston earthquake to the bedrock beneath the site and its deconvolution to the surface. The generated acceleration time history of the input earthquake is shown in Figure 4.3.2. In the same figure, the response spectrum of the input earthquake is plotted along with the Reg. 1.60 spectrum. It is seen that the Reg. 1.60 spectrum envelopes the Charleston earthquake for most of the frequency range.

While the criteria for the stability of the Par Pond Dam will be based on the response of the dam to the Charleston-like earthquake, seismic analysis will also be performed using the Reg. 1.60 earthquake family in order to assess the difference in response between different earthquakes. For a probabilistic analysis which can be performed on the structure the simulated earthquakes will be deduced from the relation

$$g(t) = 2\zeta(t) \sum_{i=1}^{N} \overline{\Phi_a(\omega_i)\Delta\omega} cos(\omega_i t + \phi_i) \qquad (4.3.6)$$

where $\phi_i$ is a vector of random phase angles uniformly distributed between 0 and $2\pi$, $\Phi_a(\omega)$ is the power spectral density and $\zeta(t)$ is a nonstationary modulating function. The earthquake input belonging to the Reg.1.60 family and used in this deterministic analysis was generated from the above relation.

Since the POROSLAM program operates in the frequency domain, the Fourier series expansion of the Charleston-like earthquake was introduced as base excitation of the embankment/foundation system.

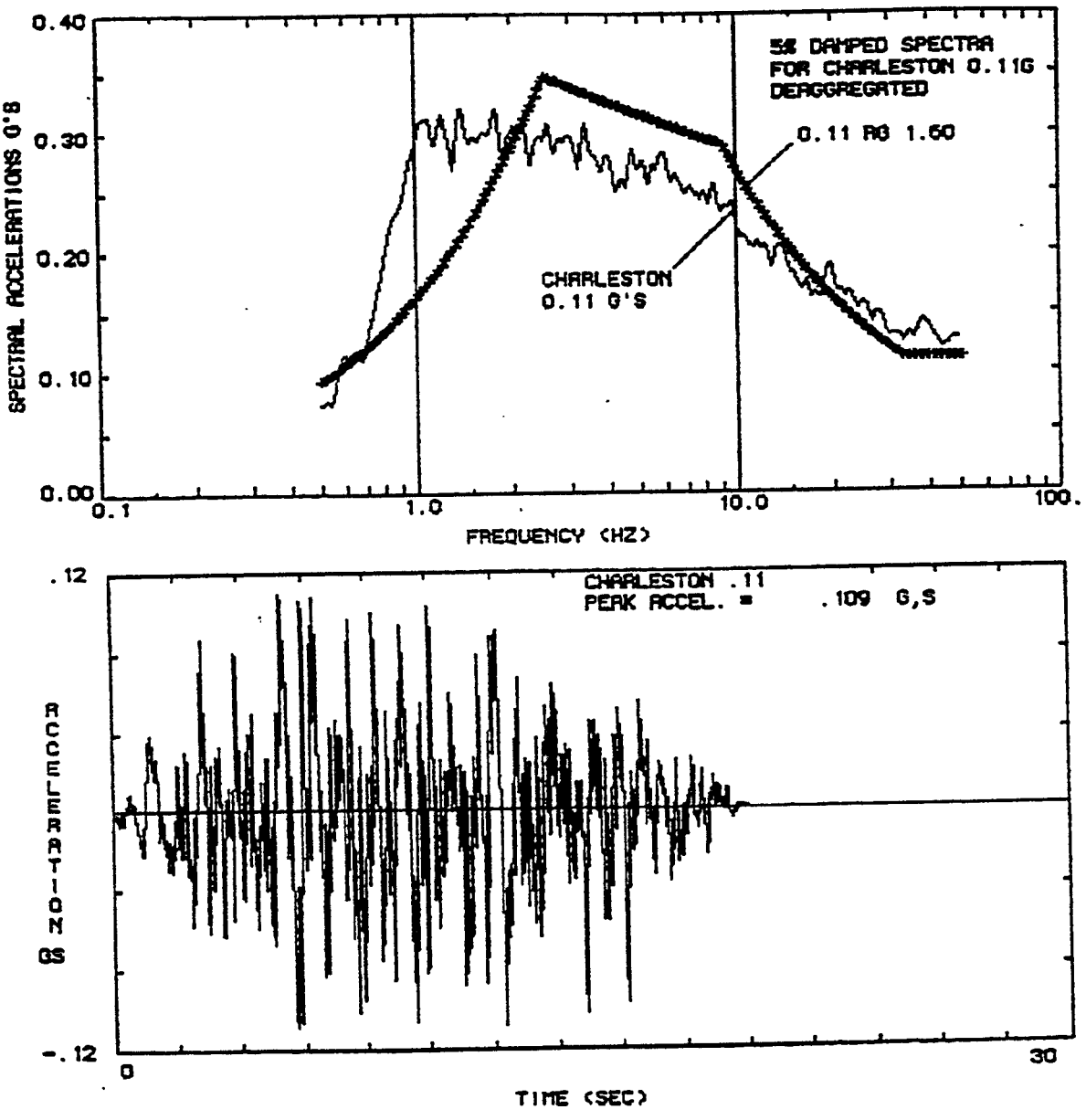


**Figure 4.3.2** Response Spectra of Charleston-like Earthquake Generated Ground Acceleration.

The application of the input earthquake at the bottom of the model rather than the ground surface was considered a conservative measure. However, in order to eliminate the possibility that there is a drastic change in the response of the dam caused by altering of the ground motion as it travels through the soil, the free-field Charleston earthquake was deconvolved to the base of the model (about 107 feet below the surface) and then used as the input excitation.

It is apparent from the standard penetration resistance test that the foundation layers of the dam lie over firm sand strata. Consequently, the assumption of relative motion between the embankment/foundation system and the base is reasonable.

The frequency solution of the problem provided the displacement response from which the soil acceleration, the dynamic stresses and the dynamic pore pressure were evaluated. The time history of these system variables is obtained with the inverse Fast Fourier process.

### 4.3.1 Slope Stability Analysis of Par Pond Dam

One of the possible modes of failure under seismic conditions is slope sliding of the dam embankment. In such event the resisting strength of the soil is reduced over an entire plane across the embankment allowing the mass above it to move. Failure can be seen either as an embankment settlement which does not necessarily lead to total failure or as a collapse of the embankment due to large movements of soil mass.

The conditions under which slope failure can occur are dependent on the soil static stresses that already exist in the embankment, which are amplified by the earthquake, and the soil resistance.

While the focus of the analysis is the dynamic response induced by a vertically propagating shear wave, the impact of vertical P-waves is also assessed. Lastly, in an effort to subject the structure to a more realistic seismic event, simultaneous excitations in both the vertical and horizontal directions are considered.

Figure 4.3.1.1 depicts a number of potential failure surfaces. With the static and dynamic stresses available from the analysis, the factor of safety against sliding is evaluated for each surface and for the full duration of the seismic event. The safety factor is defined in terms of the stress state of

a point that lies on the failure surface and the corresponding point on the Mohr-Coulomb failure envelope. Specifically, the safety factor of a failure surface that transverses a number of finite elements is computed according to the relation,

$$SF = \frac{{}_i A_i SF_i}{{}_i A_i} \tag{4.3.1.1}$$

where $A_i$ = area of the finite element transversed by failure surface and $(SF)_i$ = safety factor for element i. The safety factor for an individual element is formed on the basis of the intergranular stress invariants $J_1$ and $J_2'$ and the Mohr-Coulomb failure envelope where,

$$-\alpha J_1 + \sqrt{J_2'} = k$$

$$J_1 = \sigma_x + \sigma_y + \sigma_z$$

$$J_2' = [(\sigma_x - \sigma_y)^2 + (\sigma_y - \sigma_z)^2 + (\sigma_z - \sigma_x)^2]/6 + \tau_{xy}^2 \tag{4.3.1.2}$$

$$k = \frac{3C}{\sqrt{9 + 12tan^2\phi}} \qquad \alpha = \frac{tan\phi}{\sqrt{9 + 12tan^2\phi}}$$

such that

$$SF_i = \frac{k + \alpha J_1}{\sqrt{J_2'}} \tag{4.3.1.3}$$

By considering an *average* safety factor as representative of the entire surface one ensures that localized collapse of the soil (viewed as a reduction of the safety factor in an individual element below 1.0) does not automatically imply failure along the entire surface.

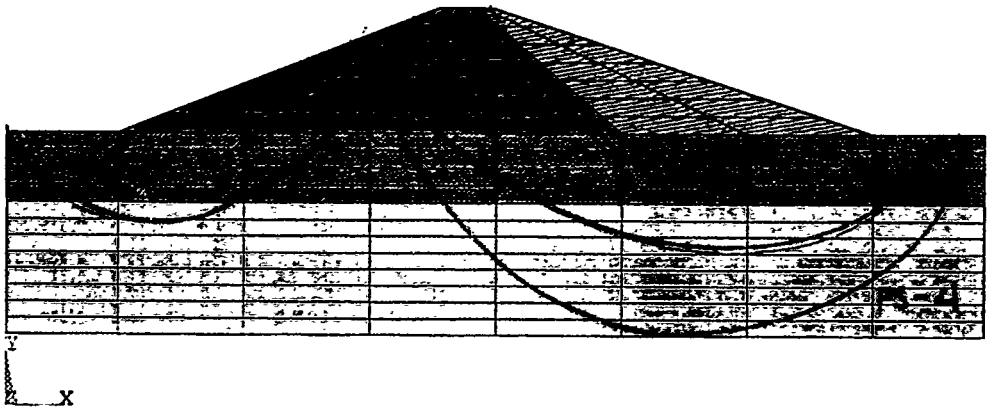


**Figure 4.3.1.1** Location of Selected Failure Surfaces.

## Factors of Safety

The REAME stability analysis provided conservative lower bound estimates for the friction angle $\phi$ in the critical layer. On the basis of the theoretical model used, for values of the friction angle equal to or greater than the lower bounds the safety factor remains above 1.0. Also from the REAME analysis it became apparent that the friction angle is the controlling soil parameter in the process. From the spectrum of values for the friction angle, two key values were selected, $\phi = 12^o$ and $\phi = 24^o$, for the safety factor evaluations with the POROSLAM program. $\phi = 12^o$ represents the lower bound case in which the safety factor drops below 1.0 for static conditions while $\phi = 24^o$ corresponds to that condition for dynamic excitation (0.10 g earthquake). These values are estimated based on the REAME results. Estimates of the safety factors for all the potential failure surfaces and the two key friction angles are presented.

Under steady state conditions and identical soil properties the REAME and POROSLAM analyses provided similar estimates of the factor of safety. Specifically, for the selected failure surface FS-4 and $\phi = 12^o$ in the critical layer, $SF_{REAME} = 0.827$ and $SF_{POROSLAM} = 0.92$. Figure 4.3.1.2 shows the variation of the safety factor for failure surface FS-4 under seismic conditions (0.11 g Charleston-like earthquake). It is apparent that the minimum safety factor is greater than 0.8 while the corresponding value determined from the REAME analysis is equal to 0.535.

A direct comparison of the minimum steady state safety factor value, as a function of $\phi$ of the critical layer, between the two analysis methods is shown in Figure 4.3.1.3.

The time variation of the safety factor over the selected surfaces is shown in Figures 4.3.1.5-10. These values are based on (a) a seismic input (0.11g Charleston-like earthquake), (b) hysteretic soil damping ($\lambda = 0.5$ percent) and (c) the specified value of $\phi$ for the critical layer. Figure 4.3.1.6 shows the effect a discretized critical layer (weak and stiff sublayers) has on the safety factor. Also shown is the estimated safety factor for the case when the bottom two layers of the finite element model have liquefied ($c = 0.0$

and $\phi = 0^o$).

Figures 4.3.1.11 and 12 depict the effect the friction angle and soil cohesion have on the safety factor against sliding. It can be seen that the changes caused by a variation of the friction angle are far greater than those caused by a variation of the cohesion. Thus, uncertainties in the friction angle of the critical layer are more critical and a sensitivity analysis for this soil property is necessary.

Based on an evaluation of the POROSLAM analysis results the following observations can be made:

a. The safety factor for steady-state conditions is above the pivotal value of **1.0**.

b. The amplification of stresses due to the seismic input (0.11g Charleston-like earthquake) causes the safety factors to fluctuate about their corresponding static value (greater than **1.0** for friction angles $\phi$ greater than $12^o$) in the weak sublayers in the critical zone.

d. If the critical layer is considered to be uniformly weak the safety factor starts to drop below 1.0 (at instances during the earthquake) for a friction angle in the layer $\phi = 20^o$, see Figure 4.3.1.3.

e. The failure surface (FS - 4) which penetrates into the lowest part of the critical layer exhibits the smallest safety factor values. This surface is critical due to the fact that liquefaction, which is more likely to occur at the bottom of the model, can result in significant reduction of the safety factor.

f. Slightly higher safety factors were obtained when the critical layer is discretized to account for variations in both the elastic properties and the friction angle.

g. The hysteretic damping in the soil also impacts on the variation of the safety factor during the earthquake. The results shown in Figures 4.3.1.2-11 are based on the dynamic stresses computed for the dam for a damping value of $\lambda = 0.5\%$ in the critical layer. The safety factor estimates for this low value of damping should be conservative.

h. The peak acceleration of the input impacts on the minimum safety factor value exhibited on the failure surface during the earthquake.

Figure 4.3.1.12 depicts this for a uniform weak layer of $\phi = 24^o$. The time variation of the safety factor for a 0.2 g earthquake and different friction angle values in the critical layer is shown in Figure 4.3.1.13. It is apparent that a 0.2 g earthquake will force the safety factor below 1.0 even for the case of a uniformly firm critical layer ($\phi = 30^o$).

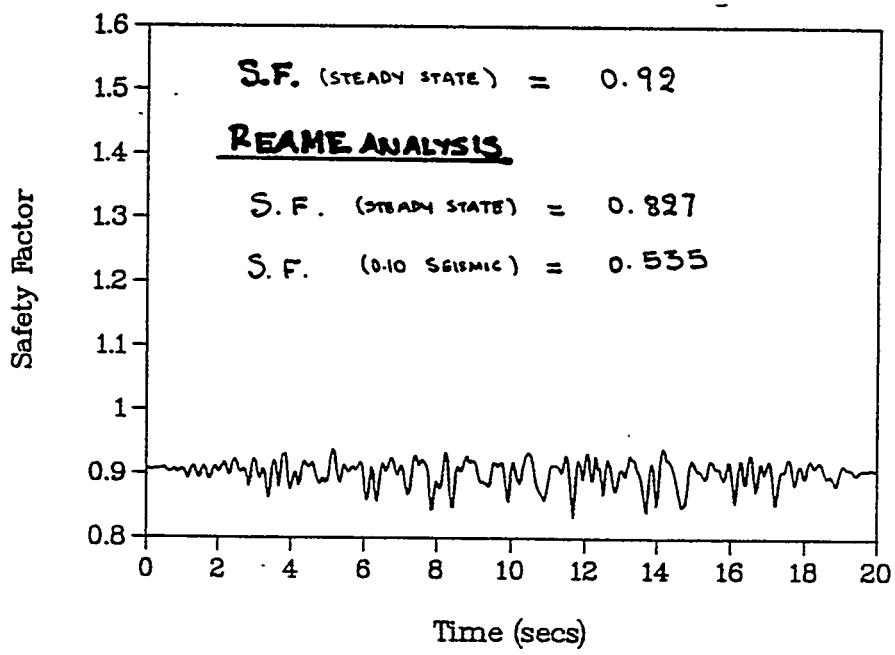


**Figure 4.3.1.2** Safety Factor Variation over FS-4 for a Uniform Critical Layer ($c = 100 \quad psf, \quad \phi = 12^o$). Comparison with Quasi-Static Results.

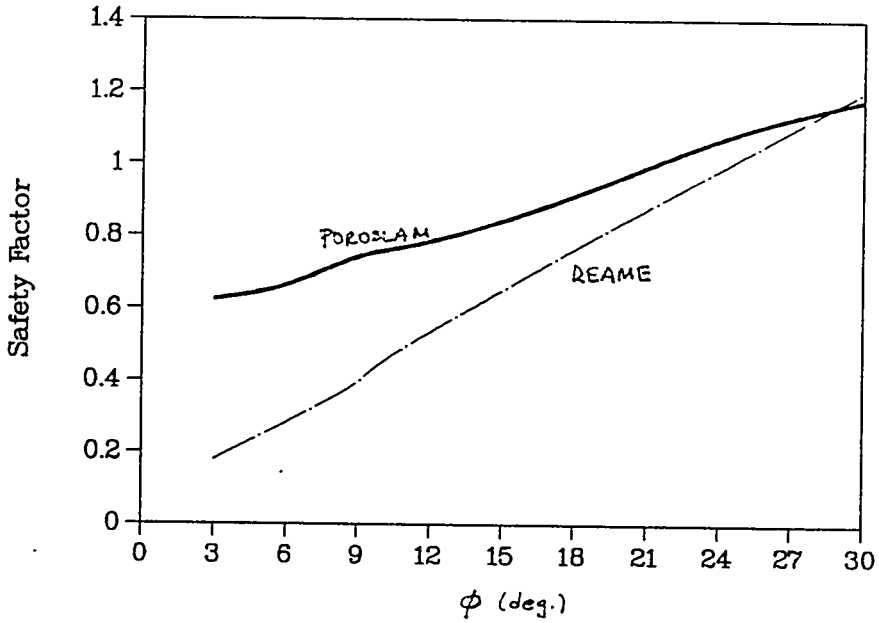


**Figure 4.3.1.3** Comparison of F.E Analysis (POROSLAM) and Quasi-Static Analysis (REAME) on Minimum Safety Factor for FS-4 and Uniform Critical Layer.

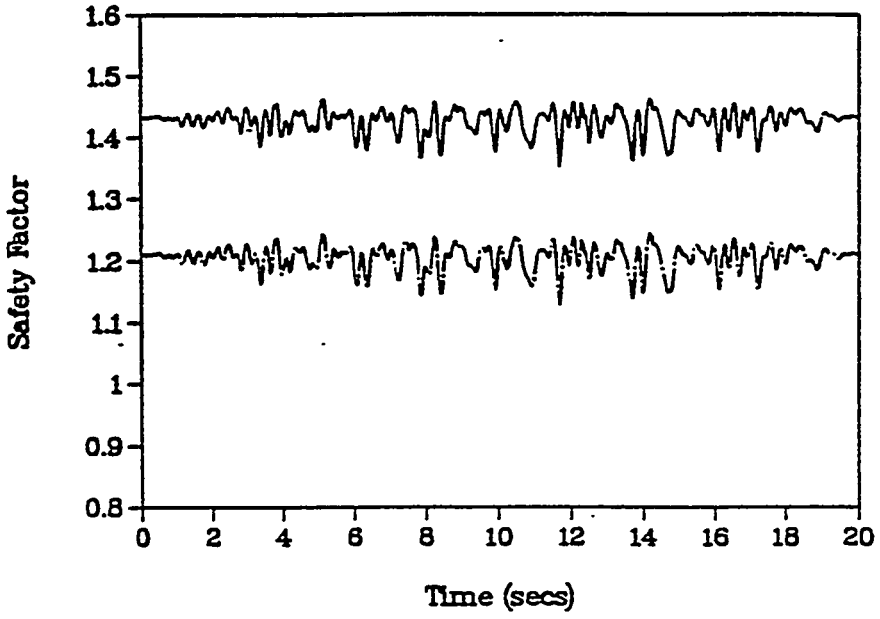


**Figure 4.3.1.4** Safety factor variation over FS-4 for a discretized critical layer (weak spot properties : $c = 100 \quad psf, \quad \phi = 24^o$). Dashed curve depicts the safety factor after liquefaction of the bottom of the critical layer has occurred.

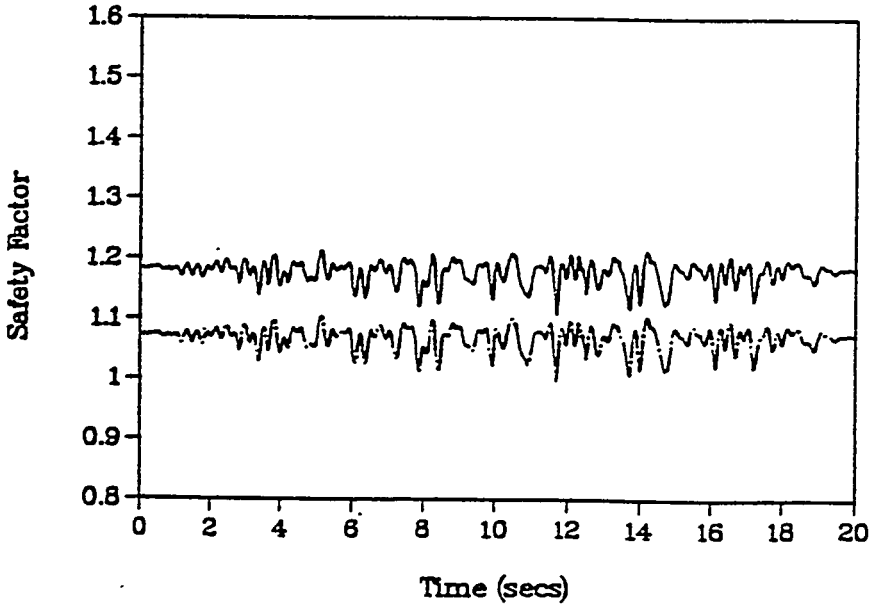


**Figure 4.3.1.5** Safety factor variation over FS-4 for a discretized critical layer (weak spot properties : $c = 100 \quad psf, \quad \phi = 12^o$). Dashed curve depicts the safety factor after liquefaction of the bottom of the critical layer has occurred.

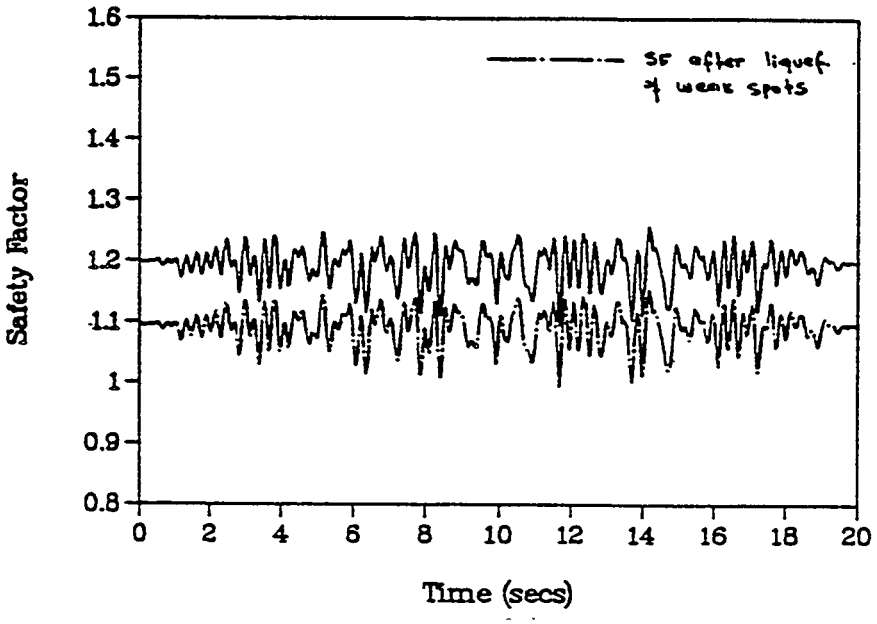


**Figure 4.3.1.6** Safety factor variation over FS-1 for a discretized critical layer (weak spot properties : $c = 100 \quad psf, \quad \phi = 12^o$). Dashed curve depicts the safety factor after liquefaction in all of the weak spots of the critical layer.

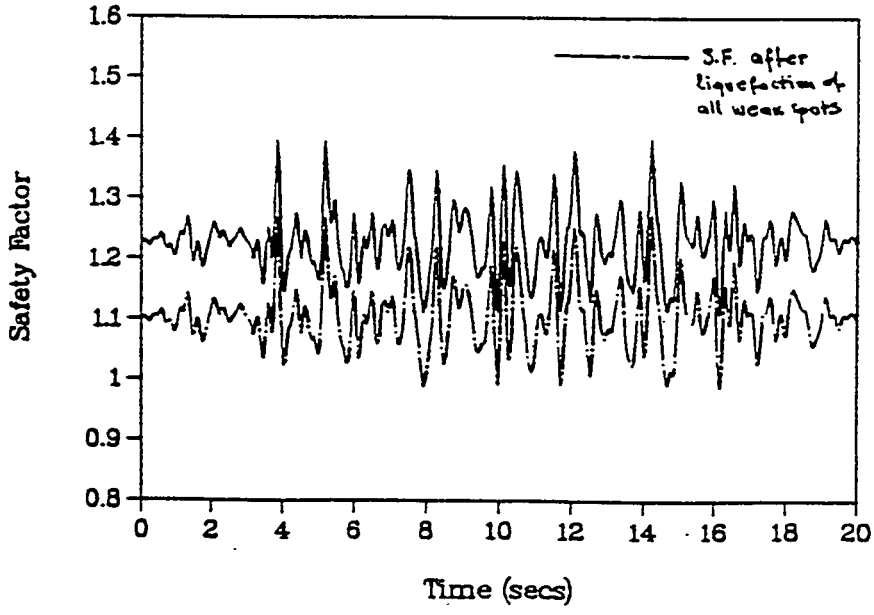


**Figure 4.3.1.7** Safety factor variation over FS-3 for a discretized critical layer (weak spot properties : $c = 100 \quad psf, \quad \phi = 12^o$). Dashed curve depicts the safety factor after liquefaction in all of the weak spots of the critical layer.

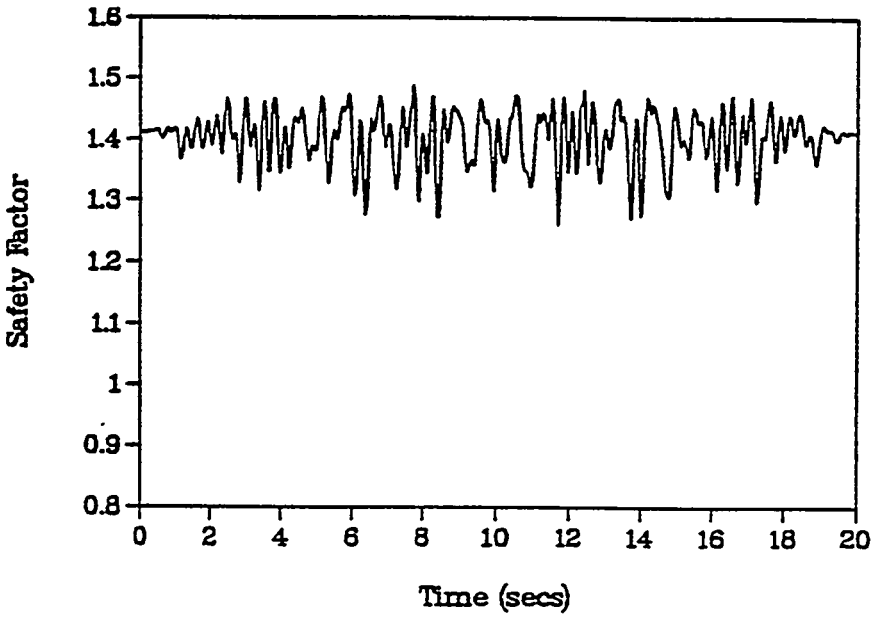


**Figure 4.3.1.8** Safety factor variation over FS-2. Failure surface does not penetrate into the critical layer.

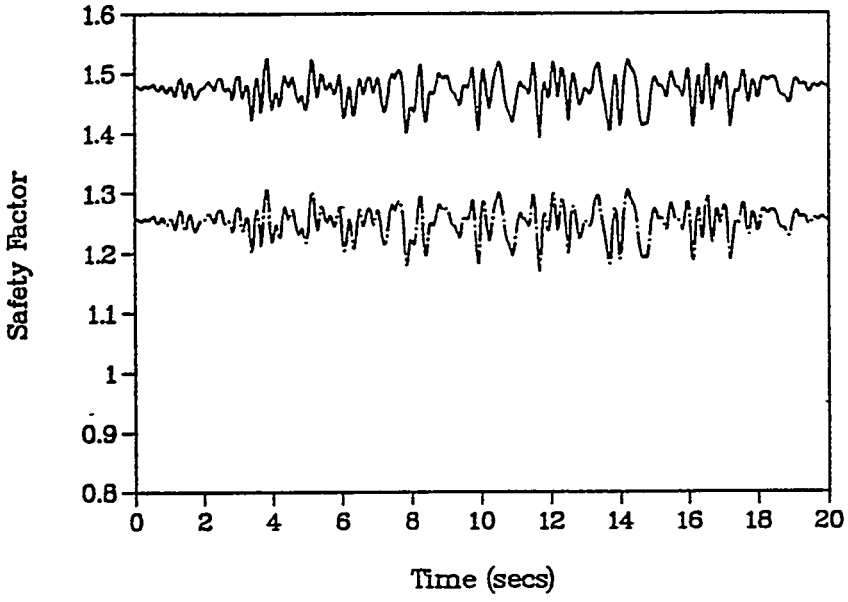


**Figure 4.3.1.9** Safety factor variation over FS-4 for a discretized critical layer (weak spot properties : $c = 100 \quad psf, \quad \phi = 24^o$). Discretization reflects both soil resistance and elastic properties. Dashed curve depicts the safety factor after liquefaction of the bottom of the critical layer has occurred.

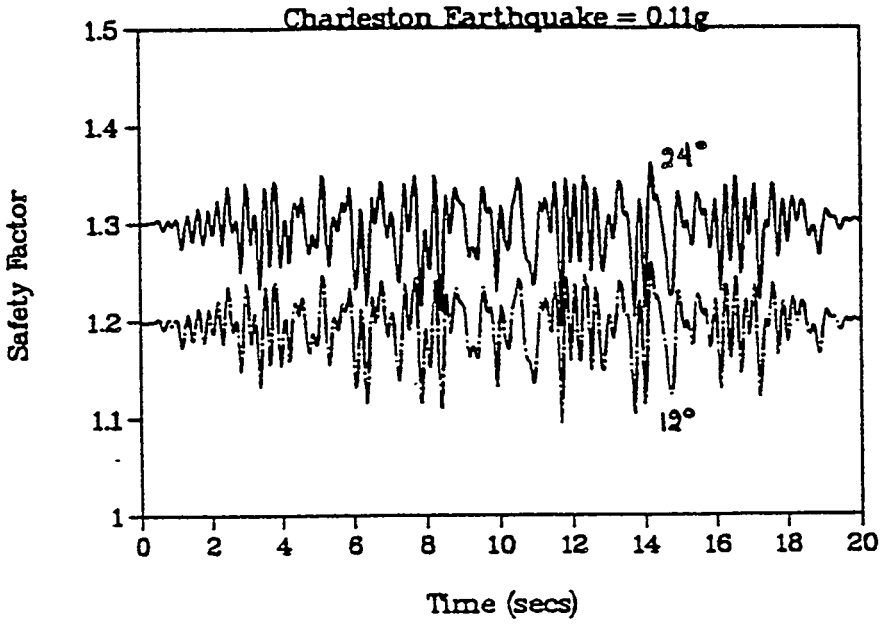


**Figure 4.3.1.10** Effect of friction angle $\phi$ variation on the safety factor of FS-1.

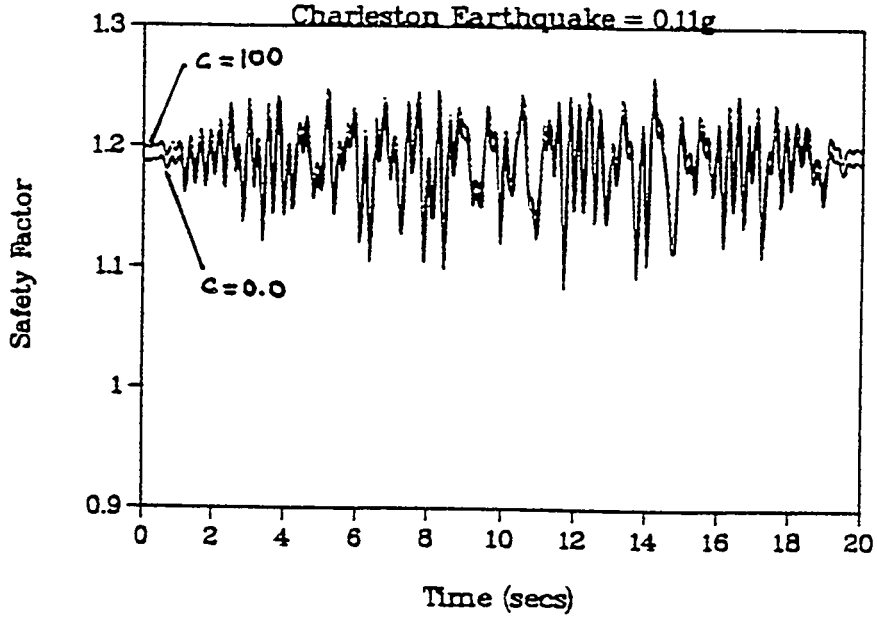


**Figure 4.3.1.11** Effect of cohesion variation on the safety factor of FS-1.

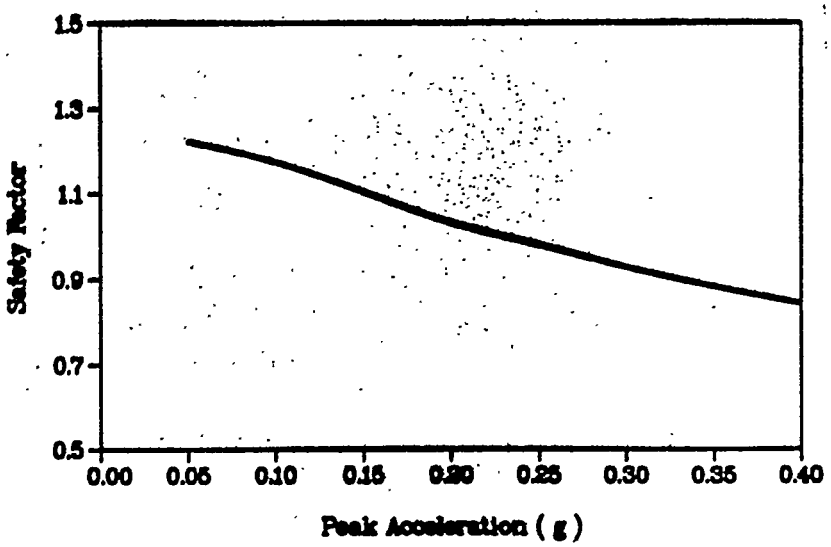


**Figure 4.3.1.12** Effect of earthquake peak acceleration on safety factor for FS-4 and Uniform Critical Layer (c = 0, $\phi = 24°$).

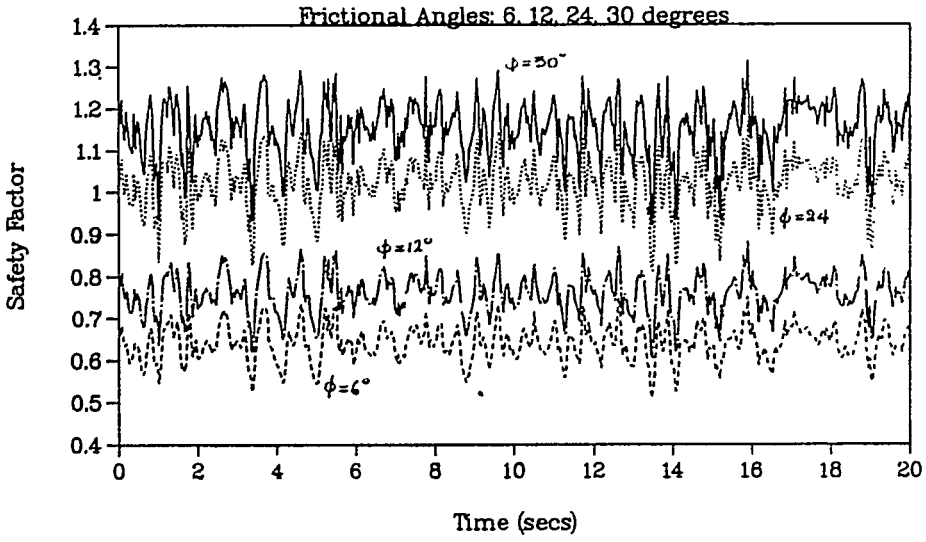


**Figure 4.3.1.13** Effect of friction angle in critical layer on safety factor for FS-4 and uniform critical layer for a 0.2 g earthquake.

**shear stresses**

While safety factors over potential failure surfaces are calculated based on the complete stress matrix (static and dynamic) the liquefaction potential of the dam is typically calculated from the dynamic shear stresses. The time variation of the shear stresses at various locations is needed to estimate the likelihood of liquefaction. The intensity of these stresses depends on the characteristics of the seismic input (response spectrum and peak acceleration) and the hysteretic damping of the soil medium.

Figures 4.3.1.14,15 depict the locations where the dynamic response of the dam has been calculated. Figures 4.3.1.16-19 show the time variation of the shear stresses at various locations and for different levels of damping. These results are the stresses induced by a vertically propagating shear wave of a 0.11 g Charleston-like earthquake. The shear stresses are maximum at the bottom of the model and reduce in the critical and foundation layers. An increase in shear stress is observed at the interface of the embankment and the upper foundation layer as a result of the embankment inertia. Slightly higher shear stresses are also observed in the lowest soft layers of the critical zone for the Model B discretization.

The difference in the dam response resulting from different earthquake families is shown in Figure 4.3.1.20. The dynamic shear stresses induced by a 0.2g Charleston-like earthquake are compared with the same stresses induced by a 0.2g earthquake with a Reg. 1.60 response spectrum. Also shown are the stresses resulting from the combination of vertically propagating shear and P waves (P wave intensity = 2/3 SH intensity) that have been generated from the Reg. 1.60 spectrum. It is apparent that the shear stresses remain relatively unchanged in the lower foundation layer when the P waves are considered. The shear stress field, however, changes drastically in the upper foundation and the embankment. The resulting increase in the shear stresses indicates that the simultaneous incidence of seismic waves must be further addressed since this case represents a more realistic earthquake event.

The variation of the peak shear with elevation at different damping levels of the critical zone is shown in Figure 4.3.1.21.

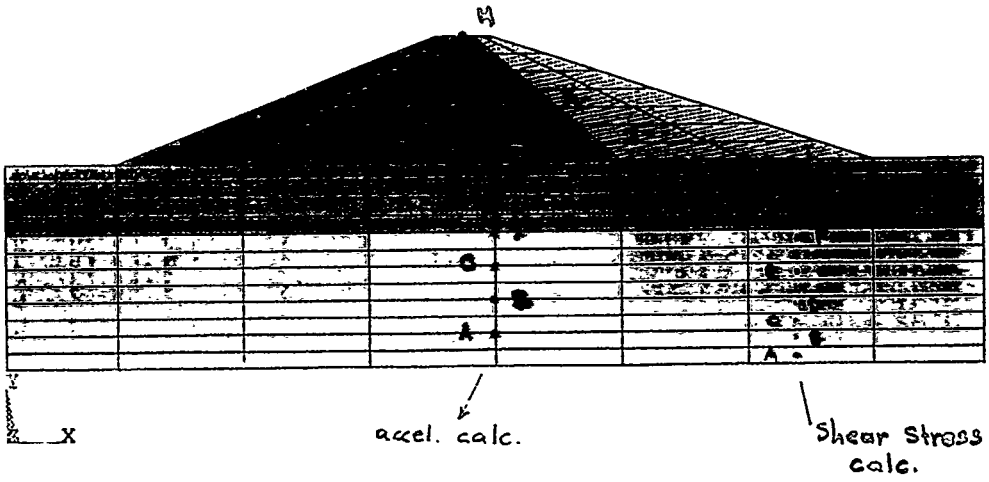


**Figure 4.3.1.14** Locations of shear stress and soil acceleration evaluation for SH waves

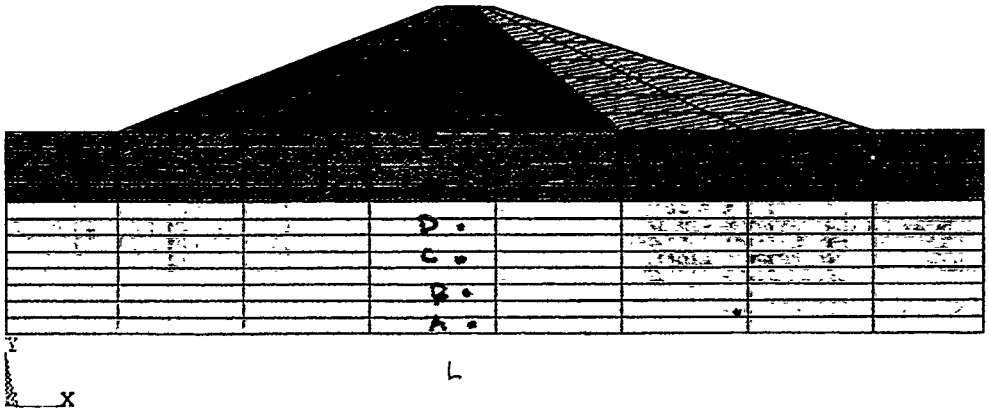


**Figure 4.3.1.14** Locations of shear stress, soil acceleration and pore pressure evaluation for (SH + P) and P waves

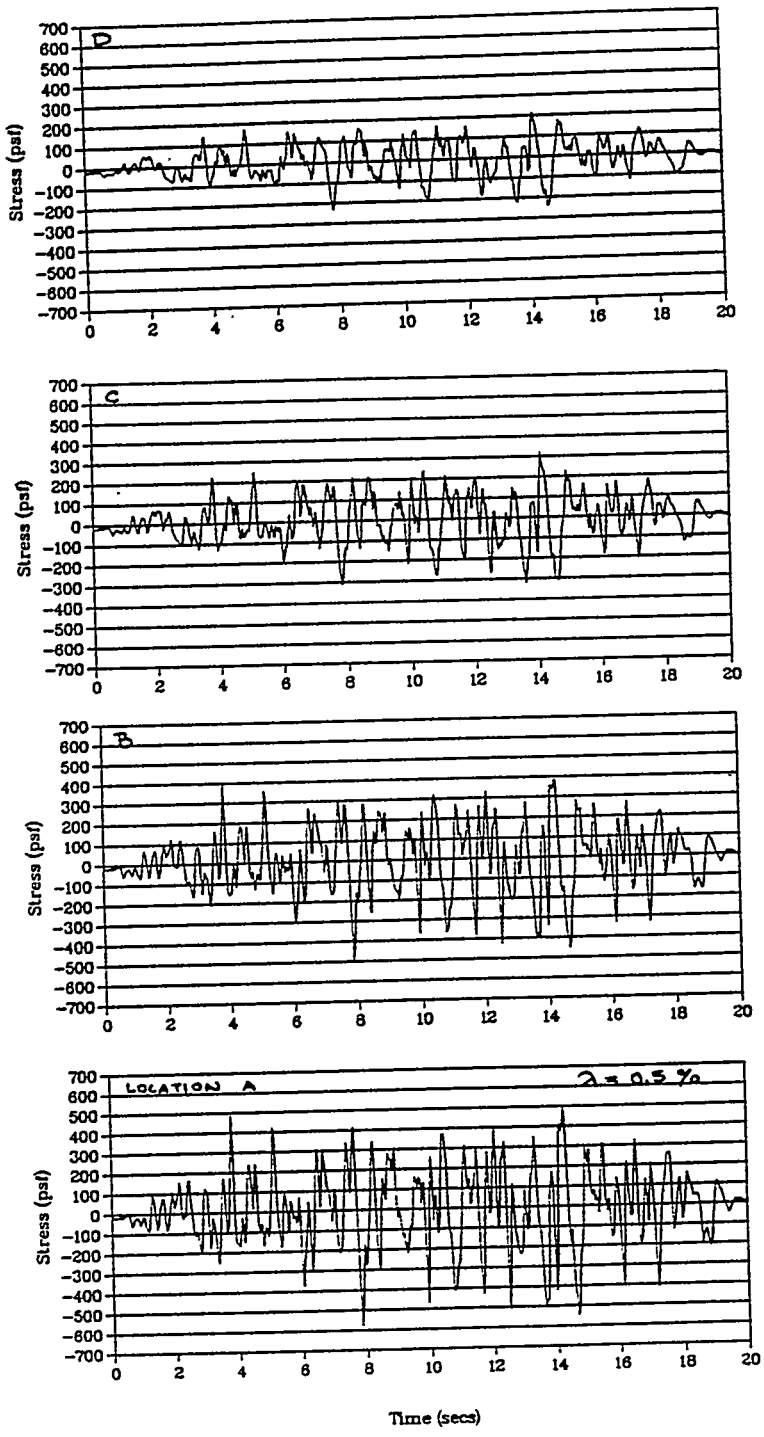


**Figure 4.3.1.16** Dynamic shear stresses for $\lambda = 0.5\%$ in the critical layer.

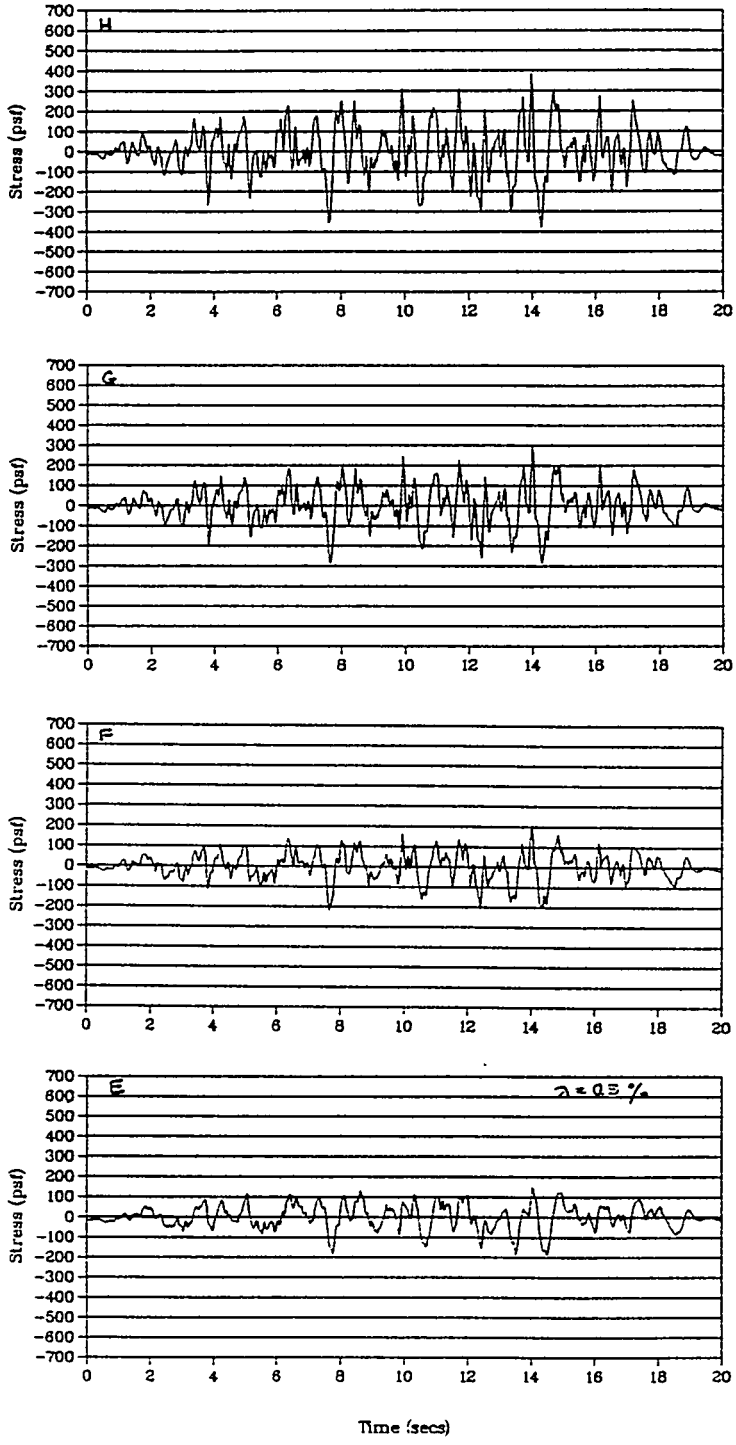


**Figure 4.3.1.16 cont.** Dynamic shear stresses for $\lambda = 0.5\%$ in the critical layer.

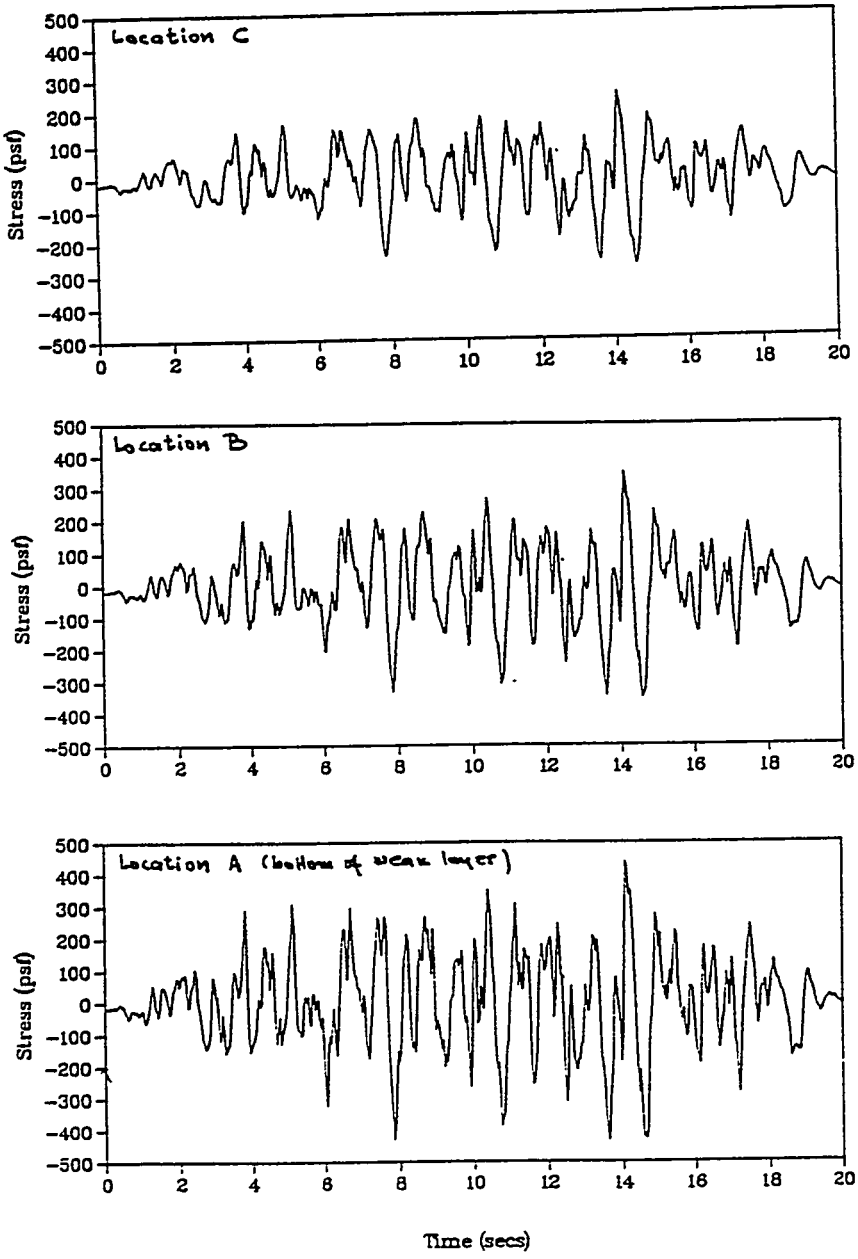


**Figure 4.3.1.17** Dynamic shear stresses for $\lambda = 1.0\%$ in the critical layer.

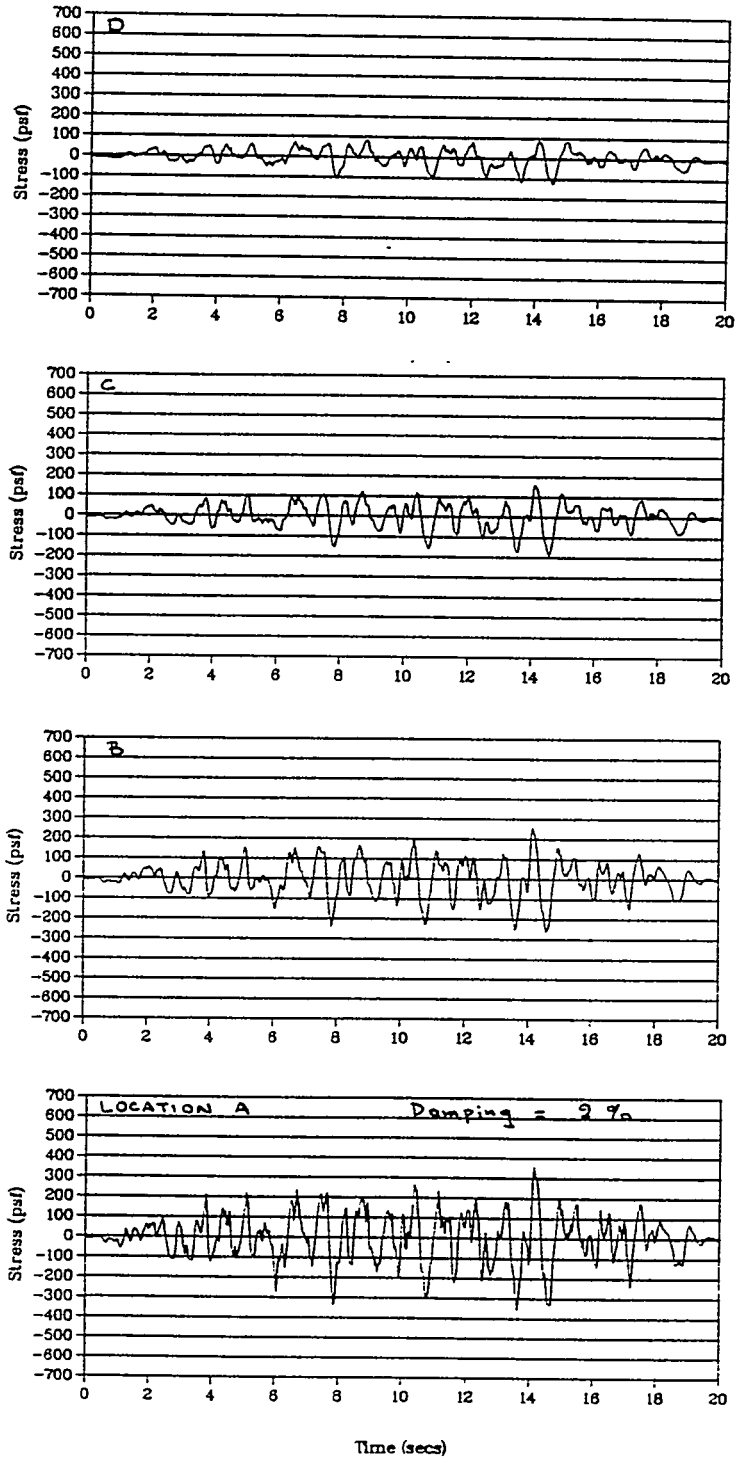


**Figure 4.3.1.18** Dynamic shear stresses for $\lambda = 2.0\%$ in the critical layer.

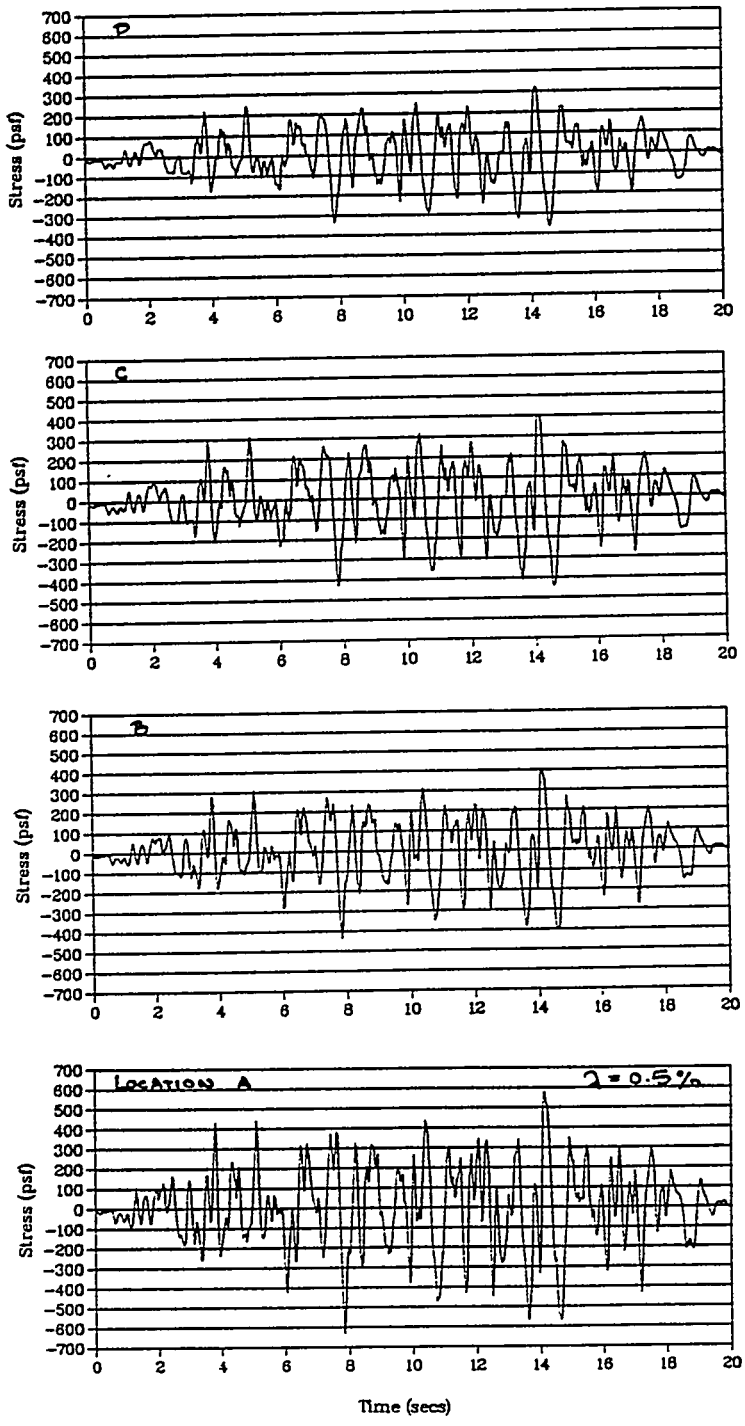


**Figure 4.3.1.19** Dynamic shear stresses for $\lambda = 0.5\%$ in the discretized (Model B) critical layer.

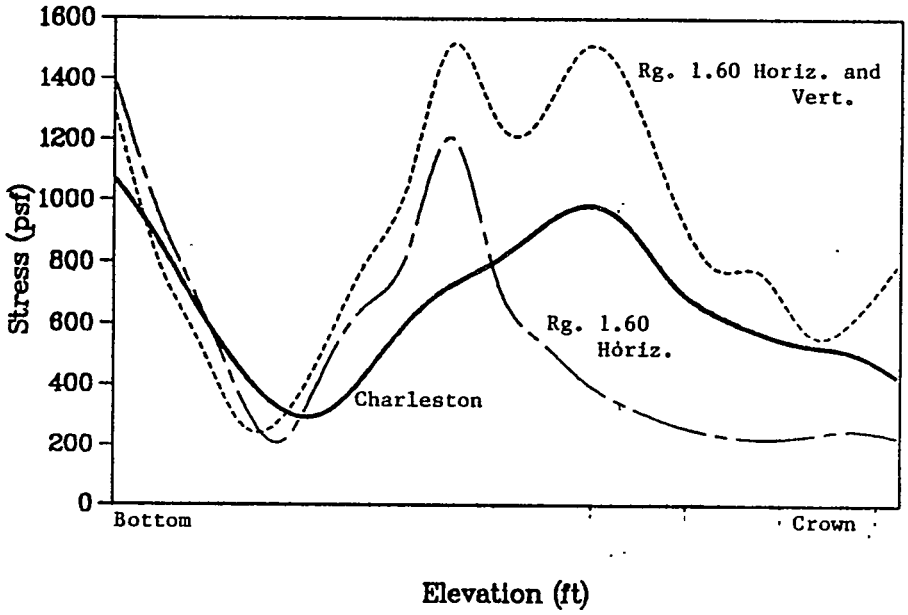


**Figure 4.3.1.20** Effect of various ground motions on maximum dynamic shear stresses.

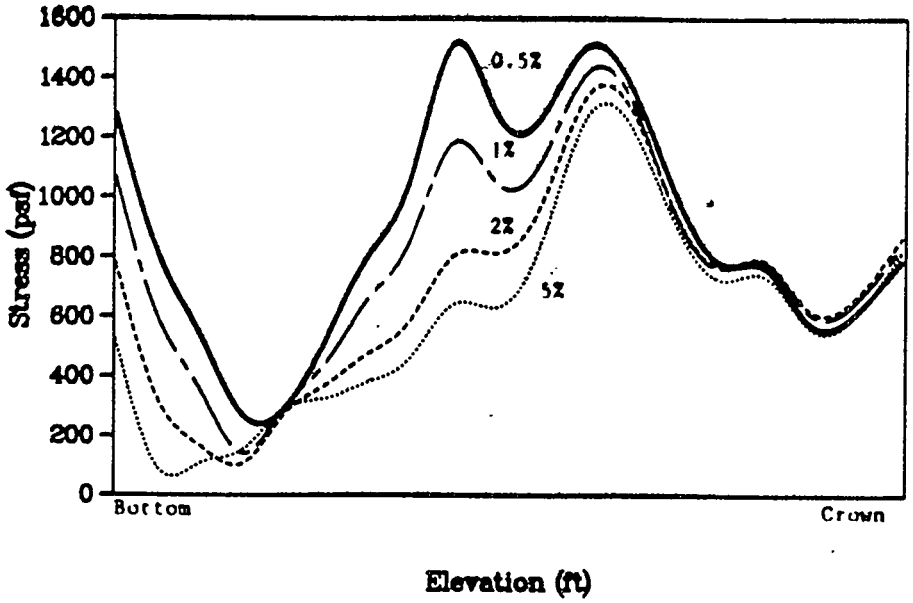


**Figure 4.3.1.21** Effect of damping on dynamic shear stresses.

### soil acceleration

The amplification of the base acceleration for the vertically propagating shear waves is depicted in Figure 4.3.1.22 for different levels of damping. The *critical* layer is clearly identifiable from the plot of the acceleration response.

### Deconvolved Surface Acceleration

The response estimates of the Par Pond Dam have been based on applying the 0.11g Charleston-like earthquake directly to the bottom of the weak layer as base excitation. To assess the change in the response of the dam due to excitation resulting from the deconvolved surface acceleration, the input earthquake was deconvolved to 107 feet (bottom of weak layer), see Figure 4.3.1.23. It is apparent that the deconvolved earthquake has a lower peak acceleration. The response of the dam in terms of the shear stresses for both records is shown in Figure 4.3.1.24. It is seen that the shear stresses induced by the deconvolved earthquake are smaller than the ones caused by applying the record directly at the base.

### pore pressure

For SH seismic waves the fluctuation of the the pore pressure, Figure 4.3.1.25, is expected to be small because the input is primarily a shear action imposed on the model.

### P wave seismic input

To assess the impact of the vertically propagating P wave (from the same family of Charleston-like earthquakes) a base excitation of 2/3 the intensity of the horizontal shear wave was applied.

Figure 4.3.1.26 shows the variation of the shear stresses caused by a P-wave input which, as expected, is minimal. The pore pressure, shown in Figure 4.3.1.27, however, exhibits considerable fluctuations. The vertical acceleration amplification is depicted in Figure 4.3.1.28.

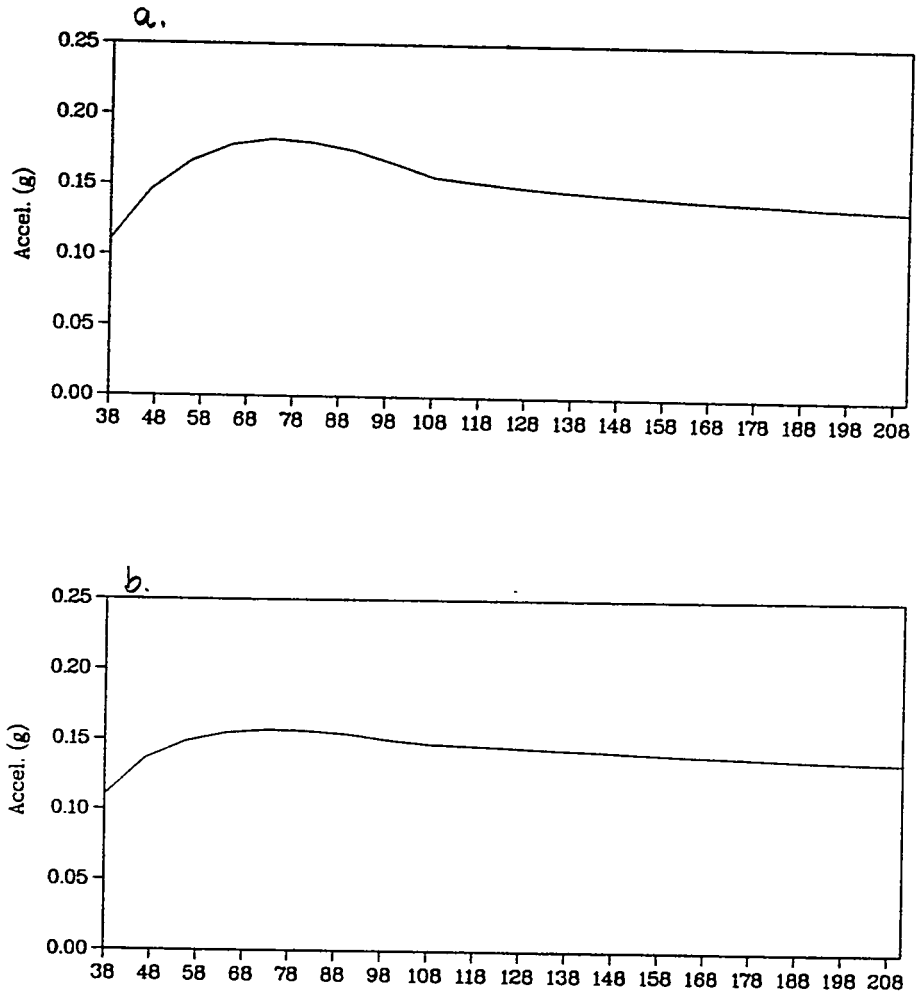


**Figure 4.3.1.22** Amplification of peak horizontal acceleration for damping $\lambda = 0.5, \quad 1\%$ in the critical layer.

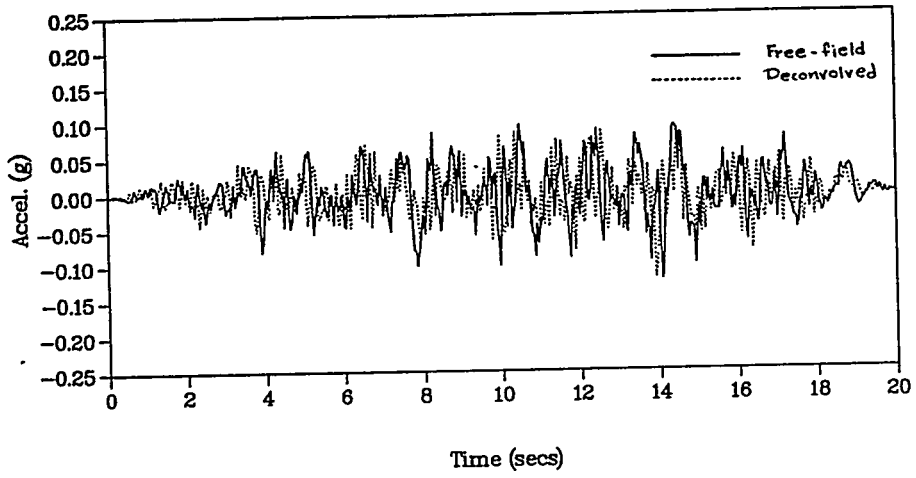


**Figure 4.3.1.23** Free-field and deconvolved 0.11g Charleston-like earthquake.

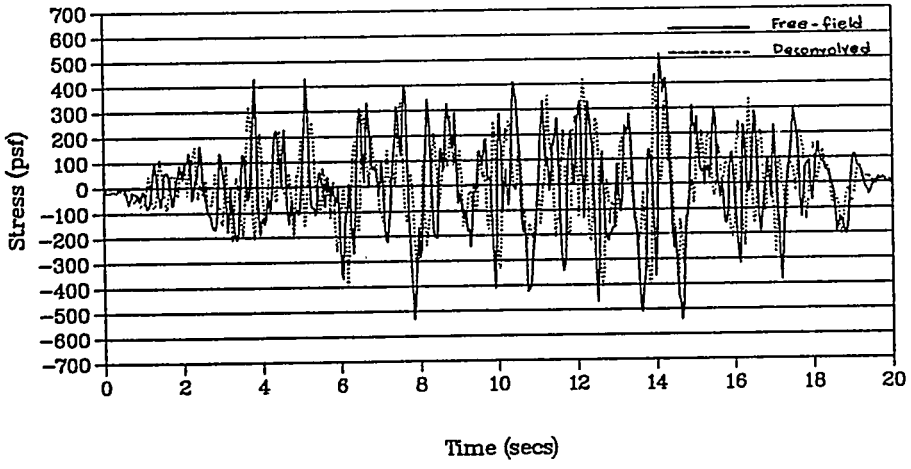


**Figure 4.3.1.24** Shear stress comparison between free-field and deconvolved ground motions.

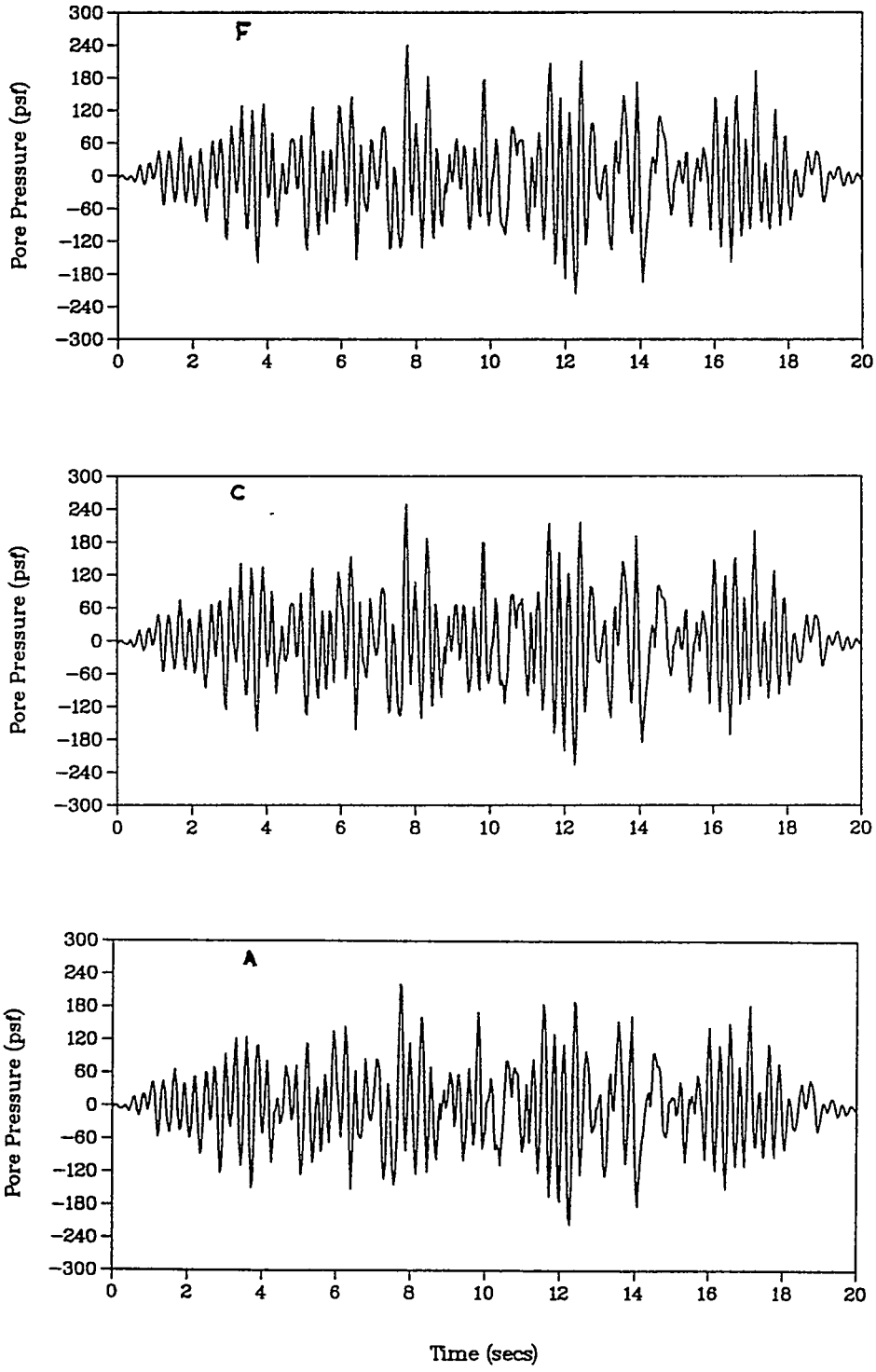


**Figure 4.3.1.25** Dynamic pore pressure induced by SH waves at various elevations.

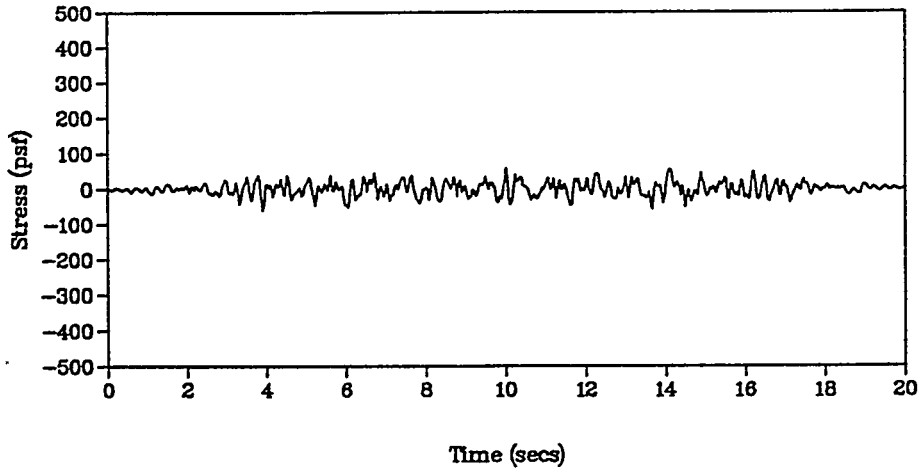


**Figure 4.3.1.26** Shear stress induced by P waves in critical layer.

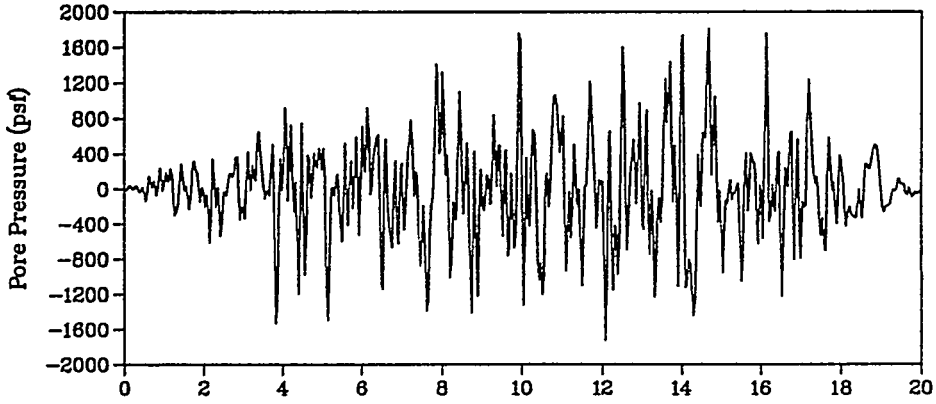


**Figure 4.3.1.27** Pore pressure induced by P waves in critical layer.

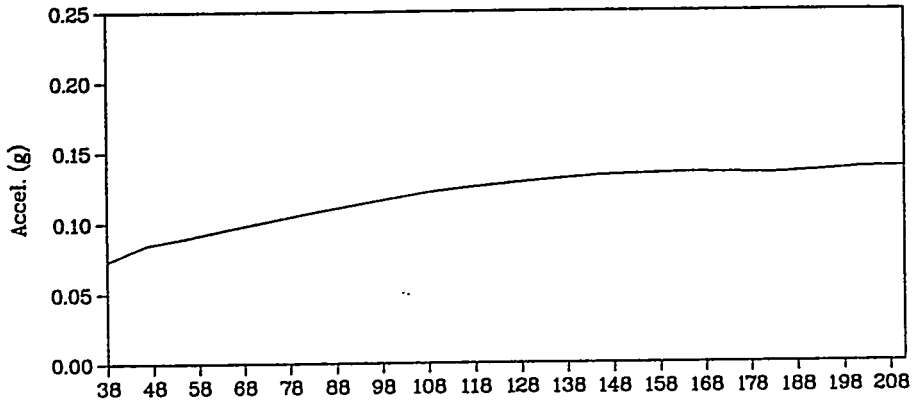


**Figure 4.3.1.28** Vertical soil acceleration amplification for P waves.

## 4.4 Liquefaction Analysis

The discovery of the *critical* layer lying beneath the stiff upper foundation layer has prompted serious concerns regarding the stability of the Par Pond Dam. The layer is identified as *critical* because of the erratic profile in the standard penetration resistance. Several locations within the layer show very low values of resistance count. The concerns are associated with the possibility of liquefaction failure trigered by an earthquake of considerable intensity and duration.

Liquefaction is a phenomenon associated with the loss of strength of a cohesionless soil during an earthquake. The mechanism is identified as one involving the movement of soil in a large deformation scenario. The soil movement can range from several feet to hundreds of feet. For a structure like the Par Pond Dam stability is dependent on the strength capacity of the soil that forms its foundation. Movement of the foundation by several feet could have serious consequences for the embankment above it.

In an effort to asses the susceptibility of the Par Pond Dam to liquefaction failure, the parameters known to influence liquefaction are estimated for the site and then used in a classical liquefaction potential evaluation. Based on laboratory tests and field observations and analysis results, the matrix of parameters influencing liquefaction was assembled. These include the characteristics of the soil type (sand, silt, clay etc.), its structure (relative density), the initial confining stress (effective stress) and the earthquake excitation (in terms of intensity and duration).

### a. soil type

It has been observed that sand deposits are more susceptible to liquefaction than deposits of silt, clay, gravel or coarse sands. This is attributed to the uniform grading of the sand as compared to the other soil types.

For the dam site and specifically for the critical zone, the bore hole samples indicate that the foundation consists primarily of stratified sands that range from clean sands to clayey sands. Consequently, a potential for liquefaction in the weak zone exists.

The susceptibility of the soil to liquefaction also depends on its void ratio or *relative density.* The looser the sand the higher the potential for liquefaction for a given earthquake. Field observations indicate that sands

of relative density 50 percent or less are candidates for liquefaction. For the soils in the embankment/foundation domain, estimates of the relative density **Dr** are derived from the standard penetration resistance field tests and the calculated effective confining stress. For the critical layer it ranged from 20 t0 40 percent.

### b. initial effective stress

It has been observed in laboratory tests that there is a direct link between the stress required to initiate liquefaction under cyclic load and the effective stress at the location of interest. Specifically, the required driving stress (or soil strength) increases with increased effective stress. The need for an accurate description of the effective stress, which is dependent on the overburden and the pore pressure, is apparent. Estimates for the effective stress were developed in the earlier sections.

### c. earthquake properties

The vulnerability of the soil to liquefaction is determined by the level of stress or strain that develops during an earthquake. For a shear stress failure the developed stress in the soil must exceed the soil strength while for a strain driven failure the threshold strain must be exceeded. The shear stresses or strains that develop in the soil are directly related to the intensity of the earthquake. In laboratory tests the soil, subjected to a cyclic load of a given intensity, fails after a number of such loading cycles. In the field and under the action of an earthquake, the event must have enough duration such that a significant number of loading cycles can develop. These cycles are not uniform of course, but the duration can be represented by an equivalent uniform cycle record.

Since the liquefaction potential is affected by the intensity, duration and character of the earthquake it is important that the excitation used in these evaluations be truly representative for the site. Further, determination of the response of the foundation and the embankment in a time history form is necessary.

## Simplified Liquefaction Procedure

For the assessment of the liquefaction potential the procedure introduced by Seed and Idriss is used. The steps of this procedure are outlined

below:

a. Define the earthquake that is likely to occur at/or in the vicinity of the site and apply as base excitation (base in this case is the firm sand below the weak layer). Since shear stress is the controlling parameter in the liquefaction process (for Seed-Idriss model), the base excitation is vertically propagating shear waves.
b. Calculate the time history record of the intergrannular shear stresses caused by the propagation of the shear waves through the embankment and the foundation layers. This evaluation of the shear stresses and their variation with time is performed for the entire domain and particularly for all locations where the stresses are expected to be high and the resistance of the soil low.
c. Transform the time history of the shear stress at the various locations in the cross section of the dam into an equivalent form. In this procedure the significant stress cycles are determined from the time history record and the number of equivalent uniform stress cycles is computed. Figure 4.4.1 depicts the transformation of the real time history record to a uniform equivalent.
d. Estimate the number of equivalent stress cycles to cause failure for each location where liquefaction is likely. This strength parameter is a property of the soil and can only be obtained from representative samples of sand from the site (or if they are not available from similar sands) reflecting the relative density of the sand, the confining pressure and the penetration resistance. The estimate of shear stress that can cause liquefaction at a particular depth (or location) is then compared against the dynamically induced shear stress (in the form of equivalent uniform stress cycles) and the potential for liquefaction is calculated.

For the evaluation of the potential for slope sliding failure a 0.11g Charleston-like earthquake representative for the site was selected and used as excitation to the model. The seismic record was (a) applied directly to the base of the model or (b) deconvolved to 107 feet below the ground surface and then applied as base motion. It was observed that the deconvolution of the free-field earthquake led to a reduction of the dynamic shear stresses.

The response of the dam for the direct base excitation was evaluated at a number of locations within the weak zone as well as in the upper foundation layer and embankment. Shear stress results are shown in Figures 4.3.1.16-21. The shear stresses are greater at the bottom of the weak layer where peak values reach **600 psf** for **0.5 %** damping. The peak values reduce to approximately **340 psf** for **2.0 %** damping.

The evaluation of the liquefaction potential is based on a process where the induced shear stresses in the field are compared to the stresses required to cause liquefaction in laboratory tests.

The induced shear stresses are in the form of series of cycles with variable amplitude while the laboratory stress tests are conducted using constant amplitude stress cycles. The soil specimen fails after a certain number of these stress cycles. The two sets of information (seismic shear stress and laboratory strength) are correlated with the transformation of the field stresses into an equivalent set of uniform cycles. This transformation makes the direct comparison of field and laboratory data possible (Figure 4.4.1). Various weighting procedures have been developed to convert any irregular stress records to a uniform one.

According to Seed and Idriss (Ref. 8), a simplified procedure that links the different magnitude earthquakes to an equivalent cycle representation can be expressed as follows:

| **Earthquake Magnitude** | **Equivalent Cyclic Stress** | **Equivalent Number of Uniform Cycles** |
|---|---|---|
| 7 | $0.65 \cdot \tau_{max}$ | 10 |
| $7\text{-}7\frac{1}{2}$ | $0.65 \cdot \tau_{max}$ | 20 |
| 8 | $0.65 \cdot \tau_{max}$ | 30 |

It is also accepted that the effective peak shear stress during a dynamic event, similar to the uniform shear for liquefaction analysis, is governed by the relation

$$\tau_{eff} = 0.65 \cdot \tau_{peak} \tag{4.4.1}$$

In order to add conservatism, BNL also used a different approach to evaluate the amplitude of the uniform shear stress. Specifically, the calculated shear stresses were transformed to a **10 stress cycle equivalent record** on the basis of the dominant (amplitude wise) stress cycles. The peak cycles are averaged (7 such peaks are identified in the actual record) while and the remainder of the record assumed to contribute 3 additional cycles. The result is a uniform record of **10 cycles** with an amplitude higher than the $0.65 \cdot \tau_{max}$ value of the Seed and Idriss method.

The level of shear stress that is required to cause liquefaction of a particular soil with site-specific conditions can only be assessed through laboratory testing. A number of tests have been conducted using cyclic triaxial compression loading. These results are expressed in terms of the stress ratio $\frac{\sigma_{dc}}{2\sigma_a}$ that induces liquefaction in **10** and **30** cycles ($\sigma_{dc}$ is the cyclic deviatoric stress and $\sigma_a$ is the initial ambient pressure used to consolidate the soil sample). Figures 4.4.2,3 depict the laboratory results for sands (Ref. 8). In order to establish a common base, these results are represented by the *mean grain size* and relative density $Dr = 50$ *percent.*

The stress ratio $\frac{\tau}{\sigma_0'}$ that causes liquefaction under field conditions must be corrected to the laboratory value. In the field, the stress ratio links the shear stress that developes at a location (converted to uniform cycles) and the initial effective stress $\sigma_0'$ (associated with the overburden and pore pressure). Figure 4.4.4 provides the correction coefficient $C_r$ of the field to laboratory stress ratio.

It has also been observed that the shear stress required to initiate liquefaction is proportional to the relative density **Dr**. The test results based on 50 percent relative density can be applied for any density. Accordingly, the complete equation that relates field and laboratory soil strength information takes the form

$$(\frac{\tau}{\sigma_0'})_{D_r} = \left(\frac{\sigma_{dc}}{2\sigma_a}\right)_{D_r=50\%} \quad C_r \quad \frac{D_r}{50} \tag{4.4.2}$$

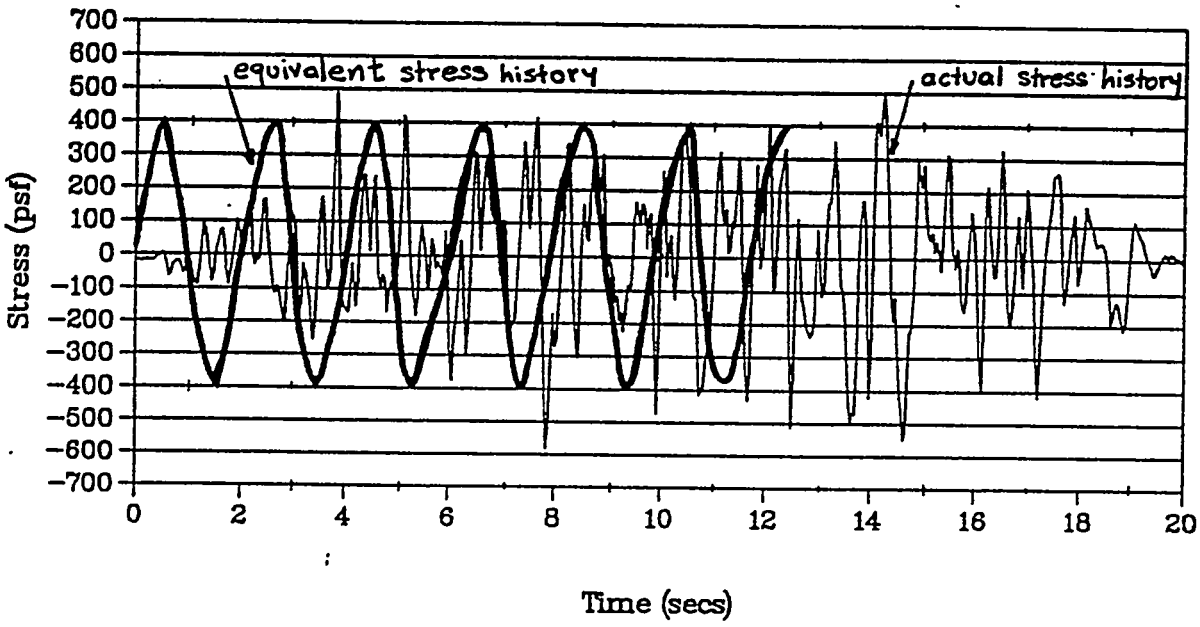


**Figure 4.4.1** Typical conversion of a stress time history to an equivalent uniform record.

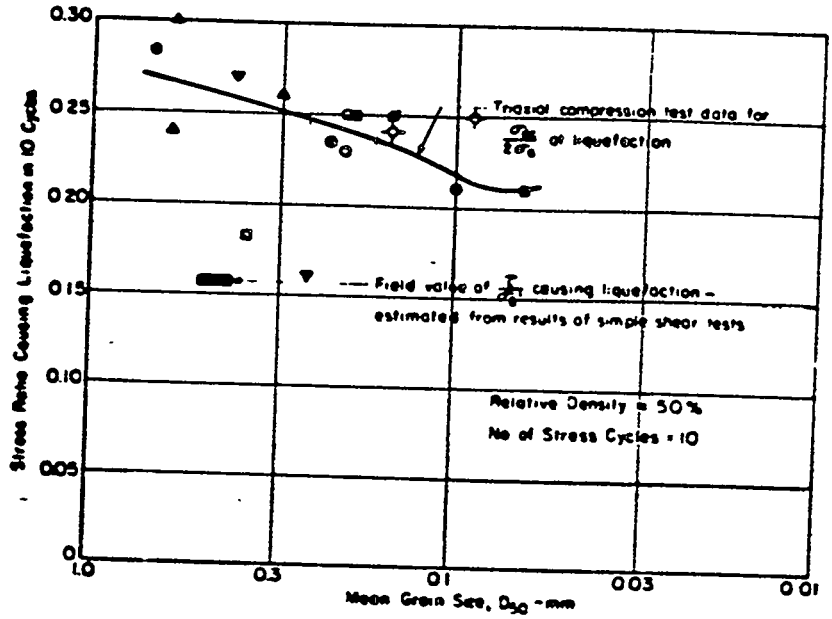


**Figure 4.4.2** Stress conditions causing liquefaction of sands in 10 cycles (Ref. 8).

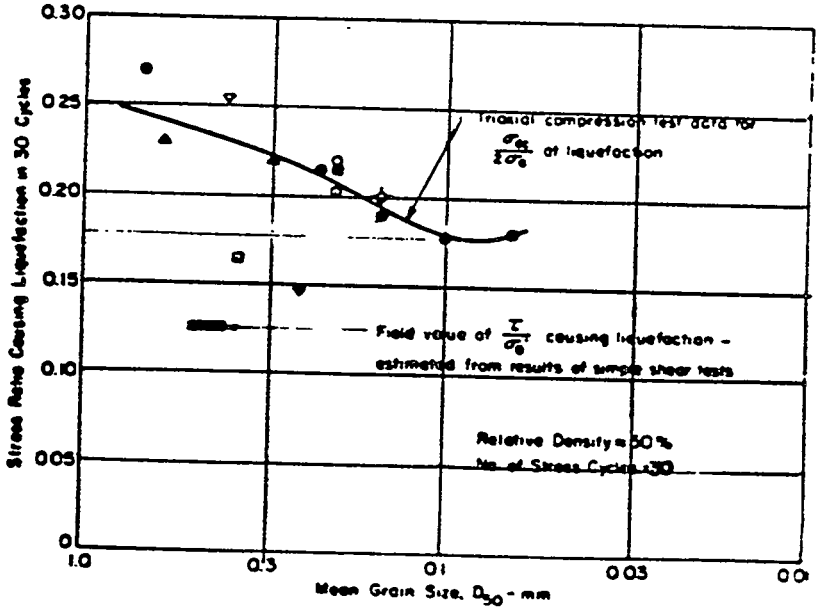


**Figure 4.4.3** Stress conditions causing liquefaction of sands in 30 cycles (Ref. 8).

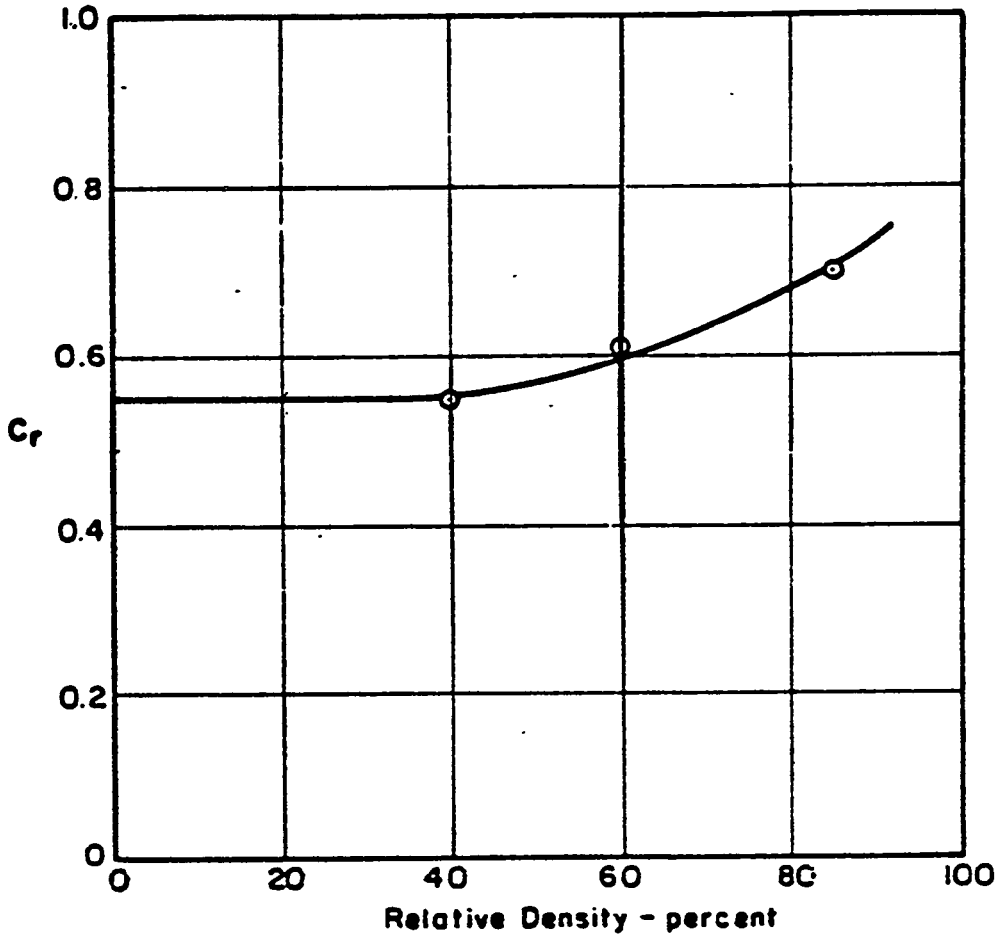


**Figure 4.4.4** Relation of correction coefficient $C_r$ with the relative density $D_r$ of sand.

The correlation of laboratory test data with the soil condition in the field described above is applied to the Par Pond Dam. The evaluation of the dam susceptibility to liquefaction requires the extrapolation of the site specific soil parameters from the various tests with results on similar soils and the calculated seismic stresses. Specifically:

- The shear stress profile (from the seismic analysis) is converted to equivalent **10** uniform cycles with both the $0.65 \cdot \tau_{max}$ approach and also the more conservative approach.

- The threshold shear $\tau$ that causes liquefaction is calculated from equation (4.4.2) and compared to the shear amplitude from the uniform cycle wave.

As seen from equation (4.4.2) the threshold shear is a function of the *effective stress* $\sigma_0^{'}$ and the relative density $D_r$. The effective stress $\sigma_0^{'}$ is calculated from the seepage and static stress analyses. The relative density profile in the dam is estimated from the field Standard Penetration Resistance test results and the existing effective stress field. Figure 4.4.5 relates the effective stress and the SPR (in blows/foot) with the relative density **Dr** of sands. Table 4.4.1 depicts the variation of the overburden $\sigma_v$, the pore pressure, the effective stress, the blow count and the relative density as a function of depth in the dam.

It should be emphasized that the available information on the liquefaction of sands is applicable to homogeneous horizontal layers subjected to shear waves. These correlations can safely be used in the study of the liquefaction of the critical zone. For the evaluation of the liquefaction potential under a complex state of stress the critical stress invariant $\overline{J_2^{'}}$ can be estimated from similar laboratory tests and compared with the one resulting from the analysis. In the case of the dam such an approach will lead to a more realistic assessment of the liquefaction potential of the embankment.

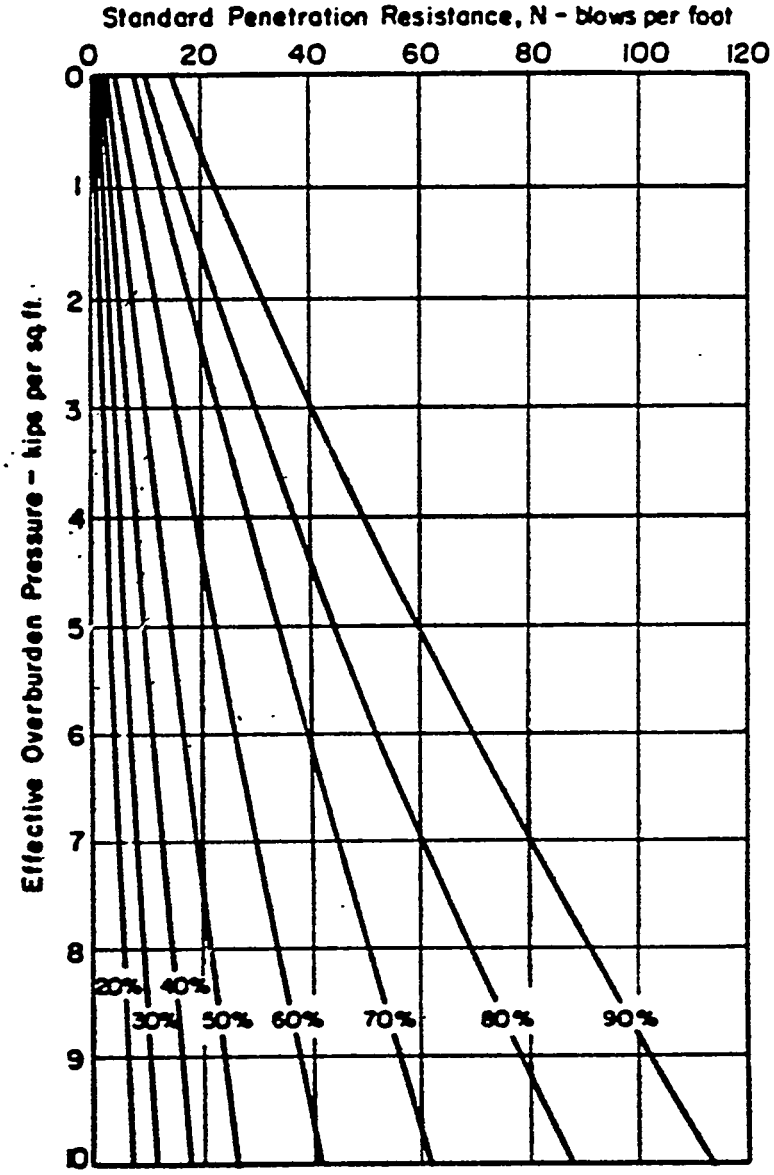


**Figure 4.4.5** Relation of $\sigma_0^{'}$ with $SPR_N$ and relative density $D_r$.

**Table 4.4.1**

| elevation (ft) | SPR (blows/ft) | $\sigma_v$ (psf) | $p_f^0$ (psf) | $\sigma_0^{'}$ (psf) | $D_r$ % |
|---|---|---|---|---|---|
| 42.3 | 14 | 16920 | 8265 | 8655 | 35 |
| 51.1 | 3 | 15742 | 7714 | 8028 | 20 |
| 59.8 | 10 | 14681 | 7157 | 7524 | 30 |
| 68.6 | 10 | 13740 | 6594 | 7146 | 30 |
| 77.3 | 24 | 12798 | 6026 | 6772 | 55 |
| 86.1 | 20 | 11734 | 5453 | 6281 | 55 |
| 94.8 | 10 | 10668 | 4875 | 5793 | 40 |
| 103.6 | 24 | 9731 | 4293 | 5438 | 55 |
| 112.6 | 60 | 8633 | 3694 | 4939 | 75 |
| 121.8 | 40 | 7375 | 3083 | 4292 | 80 |
| 131.1 | 40 | 6128 | 2492 | 3636 | 84 |
| 140.3 | 40 | 4867 | 1954 | 2913 | 90 |

The liquefaction potential can be expressed in the form,

$$LQF = \frac{Shear \quad strength \quad for \quad N_{equiv} \quad stress \quad cycles \quad (\tau)}{Maximum \quad cyclic \quad shear \quad stress \quad (0.65\tau_{max})}$$

for the shear mode, or equivalently

$$LQF = \frac{\sqrt{J'_{2\,soil \quad testing}}}{\sqrt{J'_{2\,seismically \quad induced}}} \tag{4.4.3}$$

for the complex stress state, ($LQF > 1.0$ : no liquefaction).

Based on the evaluation of the $LQF$ over the dam cross section the following observations are made concerning the susceptibility to liquefaction:

With the most conservative estimates of (1) induced shear stress, (2) mean relative density and (3) the grain size (chosen on the basis of minimum required threshold shear) liquefaction may occur **only** at the bottom of the critical layer. Figure 4.4.6 depicts the zones most susceptible to liquefaction. It also shows that the soil under the body of the embankment is stable. Liquefaction is most likely to occur under the downstream tail of the dam and possibly, but less likely, under the upstream tail. Since the sand layer under the entire embankment is expected to be homogeneous, the difference in the susceptibility to liquefaction stems from the initial effective stress profile. Effective stress $\sigma'_o$, is a controlling parameter of the liquefaction mechanism. Liquefaction is most likely at the locations of smaller effective stress (i.e. the downstream tail followed by the upstream tail).

Figure 4.4.6 shows two liquefiable zones which correspond to the two methods used to evaluate the liquefaction potential. Zone **LQZa** can potentially liquefy for a 0.11g Charleston-like earthquake if the equivalent shear stress in the uniform record is evaluated by averaging the peak shear stresses. With this approach the resulting value for driving shear is always greater than **0.65** $\tau_{max}$. Zone **LQZb** represents the locations of potential liquefaction when the amplitude of the uniform shear stresses is evaluated based on $\tau_{uniform} = 0.65 \cdot \tau_{max}$. It is apparent that zone **LQZb** does not extend to the upstream section.

The assessment to this point is based on the magnitude of dynamic shear stresses induced by the design earthquake for a damping ratio of $\lambda = 0.5\%$ in the critical layer. When the damping ratio in the critical layer

is increased to $\lambda = 2\%$, the shear stresses in the layer reduce drastically (from peak 600 psf to 340 psf) and the critical zone is no longer susceptible to liquefaction.

The present analysis shows that with conservative assumptions and using conservative analysis procedures a potential for liquefaction exists. The critical zone which, under these conditions can loose its strength during an 0.11g Charleston earthquake, lies **107 ft** below the ground surface. However, that makes it geologically old and less susceptible to liquefaction.

In the event weak spots of the critical zone liquefy, it is important to determine whether total failure of the dam can be triggered. Due to the localized character of strength loss in soil, failure can be seen as a movement of the mass above the liquefied zone along some failure surface. To assess whether the loss of strength at some location within the dam can lead to slope failure along a failure surface transversing the liquefied zone, the factor of safety against slope failure initiated by liquefaction is evaluated. This new safety factor is calculated by allowing the cohesion and the friction angle of the liquefied zones to go to zero ($\mathbf{c = 0.0\ psf}$, $\phi = 0.0$). Estimates of this new safety factor are shown in Figures 4.3.1.4-9. These results indicate that for low frictional angles in the weak sublayers of the *critical zone* and a liquefied lower section of the zone, the safety factor remains essentially above **1.0**. It should be emphasized that these results are derived using the most conservative estimates of soil properties.

The construction of a downstream berm resulted in a reduction of the liquefaction potential under the embankment toe and shifted the susceptible zone downstream. This reduction is directly related to the increase in the overburden which results in higher effective stresses in the critical zone. Figures 4.4.7,8 depict the changes in the profile of the liquefaction potential that occur for two different types of berm structure. However, the apparent positive effect has to be assessed further with a study of the behavior of the sand in the critical layer under increased confining pressure. The study must determine whether the sand contracts or not. If it contracts, then the positive effects of the berm are compromised. It should also be emphasized that only the downstream dam section benefits from the placement of a berm. For a homogeneous and susceptible lower critical zone the section under the reservoir is unaffected by the berm construction downstream.


**Figure 4.4.6** Liquefaction zones based on two methods of evaluating uniform shear stresses.

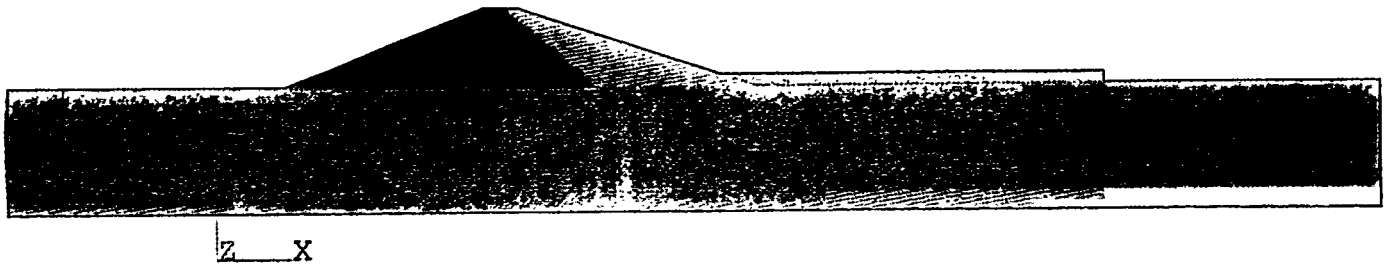


**Figure 4.4.7** Liquefaction potential profile for a small downstream berm.

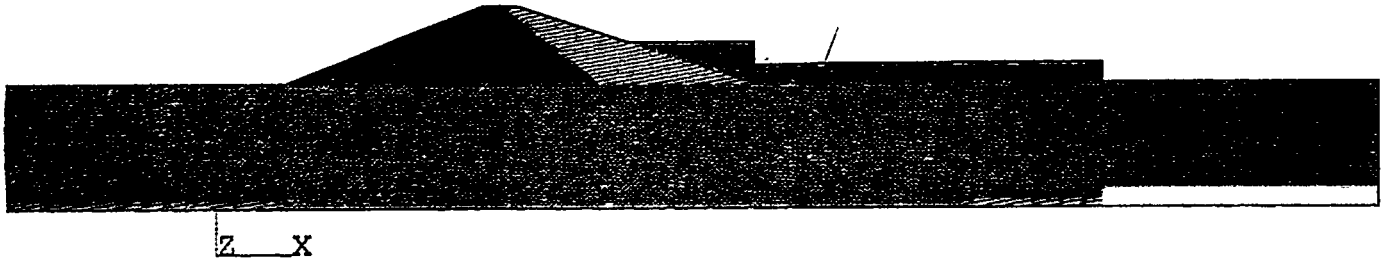


**Figure 4.4.8** Liquefaction potential profile for a large downstream berm.

# 5.0 RESULTS AND CONCLUSIONS

## 5.1 Significant Dam Safety Assessment Results

In order to arrive at a realistic estimate of the structural integrity of the Par Pond Dam, BNL has performed a detailed analysis of the static and seismic stability of the center cross section of the dam, its foundation, and surrounding soils. Specifically, the analysis included, (a) identification of potential failure mechanisms, (b) selection of a seismic input considered appropriate for the Savannah River site, (c) development of the methodologies to assess the potential failure and, (d) implementation of the methods in a unified approach to assess the factors of safety inherent in the dam/foundation system and to evaluate the merits of proposed corrective actions.

Slope failure and liquefaction were identified as the mechanisms that could lead to failure during a seismic event. The potential for failure in these two modes taken separately and coupled was evaluated to assess the safety of the dam. The results and the conclusions from the BNL analysis are summarized below:

- The strength of the in-situ soil from which the susceptibility of the section is judged is related to the friction angle $\phi$ and cohesion c. The values of these soil parameters are estimated from the available penetration resistance test results performed at the site.

- Screening analyses that are based on the stability program REAME, with the assumption of a uniformly weak soil layer (critical zone) in the lower foundation of the dam, indicated that there was a high potential for slope failure even under the action of the existing static loads. Since the dam is able to support its static loads in spite of the apparent weak zone, the REAME Code results are interpreted as very conservative. It is also probable that the assumption that the weak zone is uniformly weak is incorrect.

- A more sophisticated finite element analysis indicated that unless the critical layer is uniform and very weak (very low frictional angle $\phi$), the dam is able to withstand an earthquake of intensity **0.11g** without exhibiting slope failure. An earthquake of this level is considered

appropriate for the Savannah River site. Further, based on the limited measurements taken at the site the critical layer is not uniformly weak, and hence, the potential for slope failure is even less. Assuming the soil strengths chosen for the analysis are correct, the earthquake of intensity **0.11g** is considered an appropriate assessment of the dam capacity.

- With conservative assumptions of soil properties, (i.e., assumed low values of hysteretic soil damping), the potential for liquefaction in the critical zone is high. The liquefaction, however, is expected to occur at the bottom of the critical zone directly under the downstream toe. This zone is susceptible to liquefaction because of its relatively high induced shear stresses and smaller confining stresses. However, since the location of the liquefiable soil is about 100 feet below the ground surface, it is old geologically, and it is a small zone, it should not lead to liquefaction induced failure of the dam.

- Localized liquefaction alone does not lead to failure. Re-evaluation accounting for slope failure coupled with localized liquefaction effects was made. Even for this case, the safety factor was found to be acceptable. This result is based on a model incorporating stiff and weak subzones in the critical layer. Use of weak and stiff subzone modeling is consistent with the standard penetration resistance test results and is therefore more indicative of actual site conditions.

- With a value of 2% for the hysteretic soil damping assigned to the material in the critical zone (instead of the very conservative value of 0.5% used in the analysis), the susceptibility for liquefaction is eliminated for an earthquake with a peak level of 0.11g. Based on the computed effective strains of 0.13% obtained for 0.5%, actual hysteretic damping for the soils will be significantly higher than 2%.

- Results show that when the most conservative assumptions for soil properties are used with the most conservative evaluation procedures, liquefaction is possible under the upstream pool. However, since the confining pressure is higher upstream, the safety factor remains above 1.0 and liquefaction induced failure of the dam is not indicated.

- An analysis that incorporates both vertical and horizontal earthquake inputs, correlated in time, indicates significant increases in the em-

bankment shear stresses which reduces the safety factor against slope sliding, but does not drive it below **1.0**. Moreover, this combined earthquake does not amplify the liquefaction potential in the critical zone. It should also be noted that horizontal and vertical earthquake inputs correlated in time is not considered to be realistic. They will usually be uncorrelated in time. This case can, however, be considered as an upper bound load case.

- When a seismic input of 0.2g is considered (instead of the 0.11 g), the potential for both slope failure and liquefaction increase to unsafe levels.

## 5.2 Remedial Benefits of a Berm

The analyses have shown the PAR Pond Dam to have sufficient structural integrity to survive a credible seismic event. However, that conclusion is strongly dependent on the soil properties assigned to the critical zone. If the critical zone is assigned the most conservative (poorest) definition for soil properties, the dam seismic integrity was found to be marginal. Given the uncertainties in the properties of the soil in the critical zone, a limited study of the placement of a berm on the downstream surface of the dam, as a possible remedial action, was undertaken.

A berm improves the seismic integrity of the dam by increasing the effective static stresses in the dam/foundation system. Increased static effective stresses reduce the likelihood of liquefaction, shift the zone susceptible to liquefaction downstream and increase slope stability. Figures 4.4.7,8 show the effect of different size berms. As berm size increases, the susceptible zone shifts further downstream.

The predicted benefits of the berm are based on the assumption that the soil can support the additional load without excessive consolidation. If consolidation is great, the dam foundation system may not exhibit an effective stress increase in the critical locations and the benefits of the berm will not be realized. Needless to say, if the placement of a berm is seriously considered the competency of the soil to support its additional load must first be determined.

## 5.3 Items Requiring Further Definition and/or Clarification

Although the POROSLAM code analysis is substantially advanced from those of the REAME Code and other analytical techniques used in the industry, there are still areas of the safety evaluation, especially those pertaining to the development of a High Confidence of Low Probability of Failure (HCLPF), that need further definition and/or clarification as listed below:

- As has been stressed, the seismic integrity of the dam is strongly dependent on the properties of the soil and the extent of the weak or critical foundation layer. Recently, extensive additional soil testing of the dam/foundation system were performed. This information should be made available for review and correlation. Using this new material information a comprehensive properties matrix for the dam/foundation system will be developed. A detailed finite element model will be created consistent with the soil properties matrix to correctly characterize the dam/foundation system.

- Following an accurate definition of soil properties an other important element affecting dam seismic integrity is the exact character of the site seismic excitation. To correctly account for this, develop design earthquake incorporating site specific properties appropriate to the Par Pond. Use this as input for the new finite element model and perform dynamic analyses considering simultaneous horizontal and vertical inputs. Assess dam/foundation safety margins. Investigate the sensitivity of the safety margins to different families of earthquake inputs and evaluate the sensitivity of results to the rigid base assumptions.

- Although the onset of failure is adequately predicted with linear analysis methods, only the application of non-linear methods will allow a realistic simulation of dam response in a failure mode and an assessment of the corresponding consequences of the failure. In order to address this deficiency, incorporate the capability to account for non-linear soil behavior into the POROSLAM code. Use the updated code to obtain more realistic estimates of dam response, including pore pressure buildup and possible large deformations in the embankment, that would result from liquefaction and slope sliding.

## 6. References


1. Stability Analysis for Slopes. User's Manual on REAME and SWASE computer Programs, Y.H. Huang, 1988.
2. ANSYS Engineering Analysis Systems. Swanson Analysis Systems Inc., 1989.
3. *POROSLAM. Two-Dimensional Dynamic Solution of Elastic Saturated Porous Media*, N. Simos, C.J. Costantino, C. Miller, Earthquake Research Center, City Univ. of New York.
4. *Seismic Risk Assessment of Small Earthdams*, C.J. Costantino, N. Simos, Y.T. Gu, Technical Report NCEER-91, Earthquake Research Center, City University of New York.
5. *Engineering for Dams, Vol I*, W.P. Creager, J. D. Justin and J. Hinds, 1944.
6. *Preliminary Assessment of Par Pond Dam Seismic Stability*, GEI Consultants, Inc., 1992.
7. *Liquefaction of Soils During Earthquakes*,Committee on Earthquake Engineering *et al*, National Academy Press, 1985.
8. *A simplified Procedure for Evaluating Soil Liquefaction Potential*, H.B. Seed, I.M. Idriss, Report No. EERC 70-9, 1970.
9. *Analysis of Soil Liquefaction: Niigata Earthquake*, H.B. Seed, I.M. Idriss, Journal of Soil Mechanics and Foundations Division, pp 83-108, 1967.
10. *Evaluation of Soil Liquefaction Potential for Level Ground During Earthquakes*, NUREG-0026, 1976.
11. *Representation of Irregular Stress Time Histories by Equivalent Uniform Stress Series in Liquefaction Analyses*, California University, PB-252 635, 1975.
12. *Cyclic Stress Conditions Causing Liquefaction of Sands*, K.L. Lee, H.B. Seed, Journal of Soil Mechanics and Found. Div., No. SM1, pp.47-70, 1967.
13. *Comparison of Dynamic Analyses for Saturated Sands*, W.D.L. Finn, G.R. Martin, M.K.W. Lee, Proc. of the ASCE Geotech. Div., Vol.1, pp. 472-491, 1978.

14. *Compilation of Cyclic Triaxial Liquefaction Test Data*, J.M. Ferrito, J.B. Forest, G. Wu, Geotechnical Testing Journal, Vol 2, No.2, pp. 106-113, 1979.

15. *The Generation and Dissipation of Pore Water Pressures During Soil Liquefaction*, California University, PB-252 648, 1975.

## Acknowledgement

The authors would like to express their gratitude to a number of people who have given freely of their time and effort in helping us with this evaluation. In particular, we would like to thank Richard Serbu and Thomas McSpadden of DOE-EH for their advice on various phases of this work.